Revisit to the theoretical analysis of a classical piezoelectric cantilever energy harvester

Maoying Zhou[1] Yuhong Zhao[2]

[1] Hangzhou Dianzi University
[2] Zhejiang University

December 2, 2019

Abstract

In this paper, we investigate the classical problem for a pieozlectric cantilever energy harvester. Theoretical solution to the problem is derived and compared to the solution by other authors. Asymptotic expansions of the solution is explored in the hope of finding a plausible approximation of the problem. Dependence of the output measures upon electromechanical coupling factor is therefore studies. Some adivce are provided for the design of piezoelectric energy harvester.

1 Outline of the paper

The outline of the paper should be as follows:

- To obtain the closed form solution of the CPEH problem using the harmonic balance method
- Analyze the dependence of relative displacement function $u(z;\delta)$
- Tackling the dependence of output index χ_p and output measures $\tilde{V}_p$, $\tilde{I}_p$, and $\tilde{P}_p$ upon the electromechanical coupling factor δ and base excitation frequency f_b
- Derive the asymptotic expansion of the CPEH problem for the displacement function $u(z;\delta)$ and the output index χ_p
- Explore the approximation error of the asymptotic expansion and provide some clues to improve the performance

2 Introduction

In the past decades, renewable and sustainable energy has attracted a great deal of attention with the rapid development of our society and economy. On one hand, emerging concerns have been placed upon the limited future availability of fossil fuels. On the other hand, the growing awareness of environmental protection has posted a new challenge to develop environmentally friendly ways of energy capture and consumption. In view of these challenges, reseachers have put forwad a number of promising energy sources, such as wind energy, solar energy, nuclear energy, and etc., to tackle the problem of depleting fossil fuels. Besides, a method of extracting energy from ambient environment to power low-power electronics, namely energy harvesting, has received a lot of attentions with the prospect of partially or fully replacing batteries and creating totally sustainable electronic devices.

Numerous principles, mechanisms, implementations, and applications of energy harvesting devices have been put forward since their first appearance in the 1990s, [1, 2, 3, 4] among which the harvesting of mechanical energy enjoys the most widespread investigations. Mechanical energy harvesting can be devided into several types: electromagnetic energy harvesting, electrostatic energy harvesting, piezoelectric energy harvesting and triboelectric energy harvesting, based on the underlying physics. The focus of this manuscript is piezoelectric energy harvesting devices, which rely on the direct piezoelectric effect to convert structural vibration energy into electrical energy.

A typical piezoelectric energy harvesting device is a composite structure composed of some piezoelectric elements and a vibration transduction mechanism. The composite structure is generally attached to a host structure subject to ambient vibration. The vibration of host structure is converted to the vibration of piezoelectric elements via the vibration transduction mechanism, which is then converted into electricity via the direct piezoelectric effect. Most of the piezoelectric energy harvesting devices work in the resonant mode. The peak power is achieved when the driving frequency matches the devices resonance. [5] That is to say, frequency of the ambient vibration must match that of the piezoelectric energy harvesting device.

The transducer materials for energy conversion include PZT, PVDF and the newly emerged ferroelectric relaxors such as PMN-PT [30, 50]. They have been used in various types of structures to serve specific purposes, such as cantilever beams in transverse excitation bases [1, 16, 35] and plates (diaphragms) in pressure-loaded environments [17, 32]. The layout of electrodes on the plate's surfaces has to be carefully patterned to avoid charge cancellation [18, 41]. The design of generators based on non-resonant excitations has also received considerable recent attention [3, 37, 42, 52].

In addition to experimental researches on possible mechanisms and applications of such energy harvesters, researchers have also proposed various mathematical models to guide the design and optimization of piezoelectric energy harvesters. Although the implementation of piezoelectric energy harvesting for charging a real battery in an efficient way is much more sophisticated due to the presence of AC-to-DC (alternating current-to-direct current) conversion process [6, 7, 8], researchers have considered a resistive electrical load in the circuit to come up with a simple model for predicting the electrical outputs for a given base excitation input. The coupled problem of predicting the voltage across the resistive electrical load connected to the electrodes of a vibrating harvester under base excitation has been investigated by many authors.

The early modeling attempts of piezoelectric energy harvesters employed single-degree-of-freedom (SDOF) solutions. SDOF modeling is a convenient modeling approach since the electrical domain already consists of lumped parameters: a capacitor (due to the internal capacitance of piezoceramic) and a resistor (due to an external load resistance). Hence, the only thing required is to obtain the lumped parameters representing the mechanical domain so that the mechanical equilibrium and electrical loop equations can be coupled through the piezoelectric constitutive equations.

Although SDOF modeling gives initial insights into the problems by allowing simple expressions, it is an approximation limited to a single vibration mode and it lacks important aspects of the physical system, such as the dynamic mode shape and accurate strain distribution as well as their effects on the electrical response. Since cantilever harvesters are excited due to th motion of their base, the well-known SDOF harmonic base excitation relation taken from the elementary vibration texts has been used in the energy harvesting literature both for modeling and studying the optimization of energy harvesting. It was recently shown [18] that the traditional form of the SDOF harmonic base excitation relation may yield highly inaccurate results both for the transverse and longitudinal vibrations of cantilevered harvesters depending on the tip (proof) mass to beam / bar mass ratio. Correction factors were derived [18] to improve the predictions of SDOF electromechanical relations [15] of cantilevered harvesters under base excitation.

As an improved modeling approach, the RayleighRitz type discrete formulation derived by Hagood et al [19] (based on the generalized Hamiltons principle for electromechanical systems due to Crandall et al [20]) was employed by Sodano et al [21] and duToit et al [15] for modeling of cantilevered piezoelectric energy harvesters (based on the EulerBernoulli beam theory). The RayleighRitz solution gives a discrete model of the distributed parameter system and it is a more accurate approximation compared to SDOF modeling. In order to represent the electrical outputs analytically, Lu et al [22] used the vibration mode shapes obtained from the EulerBernoulli beam theory and the piezoelectric constitutive relation [16] that gives the electric displacement to relate the electrical outputs to the mechanical mode shape. Similar models were given by Chen et al [23] and Lin et al [24] where the electrical response is expressed in terms of the beam vibration response. The issues in these analytical modeling attempts include not considering the resonance phenomenon and modal expansion as well as oversimplified modeling of piezoelectric coupling in the beam equation as viscous damping [2224]. As shown in this work, representing the effect of piezoelectric coupling in the beam equation as viscous damping fails in predicting the coupled system dynamics of a piezoelectric energy harvester, although this approach works for certain electromagnetic energy harvesters [1]. In terms of analytical modeling, more recently, Ajitsaria et al [25] presented a bimorph cantilever model, where they attempted to combine the static sensing/actuation equations (with constant radius of curvature and a static tip force) with the dynamic EulerBernoulli beam

equation (where the radius of curvature varies) under base excitation (where there is no tip force). Thus, highly different modeling approaches have appeared in the literature during the past five years and some of them might be misleading due to weak mathematical assumptions involved [26].

Recently, Erturk and Inman [27] have presented the analytical solution to the coupled problem of a unimorph piezoelectric energy harvester configuration based on the EulerBernoulli assumptions. They obtained the coupled voltage response across the resistive load and the coupled vibration response of the harvester explicitly for harmonic base excitations in the form of translation with small rotation. The short circuit and open circuit trends and the effect of piezoelectric coupling were investigated extensively [27]. Later, Elvin and Elvin [28] have observed the convergence of the RayleighRitz type of solution formerly introduced by Hagood et al [19] to the analytical solution given by Erturk and Inman [27] when sufficient number of vibration modes is used with appropriate admissible functions.

This paper presents the application of the coupled distributed parameter solution [27] to bimorph cantilever configurations with series and parallel connections of piezoceramic layers. The steady state voltage response and vibration response expressions are derived for harmonic excitation of the base at an arbitrary excitation frequency (in the form of translation in the transverse direction with small rotation). Then, by using the complete (multi-mode) solutions, the response expressions are reduced to simple but accurate single-mode relations. The single-mode relations can be used instead of the multi-mode relations for modal excitations (i.e., for excitations around resonance) of cantilevered bimorphs since the resonance excitation is the main concern in vibration- based energy harvesting. The electromechanical FRFs that give the voltage output and vibration response-to-translational and rotational base acceleration relations are extracted from the multi-mode and single-mode solutions. Experimental validation of the analytical formulation is given for a bimorph cantilever with a tip mass. It is shown that the single-mode analytical relations proposed here are very accurate in predicting the voltage output and vibration response FRFs. The bimorph device is analyzed extensively for the short circuit and open circuit resonance frequency excitations by using different resistive loads and it is observed that the analytical model can successfully predict the coupled system dynamics.

Here in this contribution, we focus on the closed-form solution to the classical model of a piezoelectric cantilever energy harvester. Based on the Euler-Bernoulli beam model and the linear piezoelectric relations, electromechanical model of the energy harvester is established, which is then converted to a boundary value problem of ordinary differential equations using the harmonic balance method. Closed form solution of the relative displacement function of the cantilever beam as well as the output performance measures is analyzed and numerically investigated. Asymptotic expansions of the relative displacement function are calculated to obtain approximate expressions for the output index and the related output performance measures. Advices are then given in terms of the structure design and performance optimization of piezoelectric energy harvesters.

> Power harvesting refers to energy retraction from ambient surroundings and converting it into useful electric energy. With advances in wireless technology and low-power electronics, energy harvesting from environmental resources has the potential to power mobile and wireless microsystems where battery replacement is either practically impossible or prohibitively expensive [7, 26, 31, 48]. Due to the ubiquitous presence of ambient vibrations, extensive research efforts have been made for converting mechanical energy into electrical power through piezoelectric, electromagnetic and capacitive transducers [36, 40]. Amongst them, piezoelectric vibration-to-electricity converters have been viewed as being superior to other means, as they have high electromechanical coupling, no external voltage source requirement and they are particularly attractive for use in MEMS [15, 20, 40] and nanosystems [28, 38]. As a result, the use of piezoelectric materials for scavenging energy from ambient vibration sources has recently witnessed a dramatic rise for power harvesting [5, 13, 24, 25, 49, 56].
>
> A vibration-based piezoelectric energy harvesting system includes three essential components: an oscillator, a piezoelectric medium and an energy storage circuit, as demonstrated in figure 1. An oscillator is designed to transmit ambient vibrations into mechanical strain energy which is converted into electrical energy via the direct piezoelectric effect. The generated charges are accumulated through an interfacing circuit for AC/DC conversion and presented to a load circuit. Precisely, the power generator is typically designed as a resonant oscillator since the peak power is achieved when the driving frequency matches the devices resonance [40]. The transducer materials for energy

conversion include PZT, PVDF and the newly emerged ferroelectric relaxors such as PMN-PT [30, 50]. They have been used in various types of structures to serve specific purposes, such as cantilever beams in transverse excitation bases [1, 16, 35] and plates (diaphragms) in pressure-loaded environments [17, 32]. The layout of electrodes on the plates surfaces has to be carefully patterned to avoid charge cancellation [18, 41]. The design of generators based on non-resonant excitations has also received considerable recent attention [3, 37, 42, 52].

The circuit design is required for electrical compatibility and maximum power transfer to the load. It consists of AC/DC interfacing electronics connecting the piezoelectric element to the terminal electric load. Power optimization schemes therefore depend not only on the mechanical solicitation, but also on the specific types of interfacing circuits. This motivates a variety of research efforts for proposing appropriate electronic interfaces. The most common one is the standard interface which includes an AC/DC rectifier followed by a filtering capacitance, as shown in the middle of figure 1. Ottman et al [33] have studied the electrical behavior of this standard system based on the uncoupled model which simplifies the vibrating piezoelectric structure as the current source in parallel with its internal capacitance. They further developed adaptive DC/DC converters for impedance matching [34]. Shu and Lien [44] subsequently proposed an improved analysis for optimizing AC/DC power extraction without the uncoupled assumption. They also investigated the relation between electrically induced damping and conversion efficiency for a rectified piezoelectric device [45] (cf [22, 23, 39]). The result shows that optimization criteria vary according to the relative strength of electromechanical coupling to mechanical damping ratio. Guan and Liao [10, 11] analyzed the charge/discharge efficiencies for several different energy storage devices. Wu et al [54] and Wickenheiser et al [53] investigated the transient behavior of a storage capacitor under charging. Liu et al [27] used the switch-mode power electronics to develop a scheme for active energy harvesting. Based on the beam model, Huetal[14] numerically studied the interaction between the piezoelectric vibrating structure and the storage circuit.

Another recently emerged energy harvesting circuit is the synchronized switch harvesting on inductor (SSHI) interface which is added to the piezoelectric element together with the standard DC technique, as also illustrated in the middle of figure 1. This technique was proposed by Guyomar and his co-workers [2, 12, 19, 21, 29] who have shown that power is boosted significantly in a weakly coupled electromechanical system. However, the effect of frequency deviation from resonance on the electrical behavior of an SSHI system is not taken into account in the original analysis. Instead, Shu et al [46] have proposed several improved estimates for the parallel- SSHI circuit accounting for this effect. They have shown that the electrical response of a parallel-SSHI system is similar to that of a strongly coupled electromechanical standard system operated at the short circuit resonance. Furthermore, this technique improves the scavengers bandwidth significantly in comparison to the standard technique. Here, we provide another improved analysis for electrical performance evaluation of a series-SSHI system. It takes into account the full electromechanical coupling response and vibration phase- shift effect, and therefore the analysis is capable of revealing the system characteristics in the vicinity of resonance. The results show that the electrical behaviors of these two ideal SSHI systems are conjugate with each other in comparison to the standard technique. However, they exhibit a dissimilar response if the effect of diode loss is considered. It turns out the feature of wide band could be lost in practical devices endowed with series-SSHI circuits. Finally, some of our preliminary results have been reported in a conference paper [47]. Here, we systematically derive the main results with numerical validation and provide discussions concerning electrical loss in detail.

This paper is organized as follows. First a piezoelectric transducer is modeled as a lumped single-degree-of-freedom system undergoing periodic forcing in section 2. A number of research efforts based on the distributed parameter methods have been made for analyzing a vibrating piezoelectric structure connected to a single resistor [4, 8, 9, 16, 43]. They show advantages in predicting the model shapes, strain distribution and energy harvesting performance based on geometry and material properties of a structure. However, difficulties arise if the nonlinear interfacing circuits are taken into

account in analysis [14]. Limited success has been achieved by bridging structural modeling and circuit simulation such as coupled FEMSPICE models [6, 55]. Hence, if the focus is the overall electrical behavior rather than the detailed response at each specific point of a structure, the reduced model suffices the need for harvesting circuit design. Subsequently, an energy harvester using the standard circuit is introduced in section 2.1 and the electrical response of a series-SSHI system is analyzed in detail in section 2.2. The harvested power is derived and expressed explicitly in terms of several dimensionless system parameters. The operating points for achieving optimal power is also discussed there. For the purpose of comparison, the electrical behavior of a parallel-SSHI system is briefly reviewed in section 2.3. Next, the results are numerically validated in section 3.1 and are discussed under the case of non-ideal voltage inversion in section 3.2 and the case of diode loss in section 3.3. The conclusions are made in section 4.

newpage

Small-sized and lower-power-consumption wireless devices have been widely used in structural health monitoring since the replacement of batteries is inconvenient and expensive. The development of self-powered devices, which can gather ambient energy from the surroundings, is a hot issue [13]. Being renewable and widely existing in surroundings, harvesting wind energy has great application prospects in self-powered devices. The wind-induced vibration energy can be converted to electric energy by electromagnetic, electrostatic, piezoelectric and magnetostrictive energy harvesters [46]. Comparing with other energy harvesters, piezoelectric energy harvesters are the most common energy harvester, due to their high power density, wide range of frequencies, easy to miniaturize design and integration [79]. For example, Kwon [10] proposed a T-shaped piezoelectric energy harvester for generating electric power from natural fluid flow. In their work, the device consisted of a bimorph cantilever with T-shape which hastens occurrence of flutter at a low fluid speed. Bryant et al. [11] investigated the stability characteristics of aeroelastic flutter energy harvesters. Moreover, by investigating the operation of an array of aeroelastic flutter energy harvesters, Bryant et al. [12,13] demonstrated that synergistic wake interactions can increase power output of energy harvesters. McCarthy et al. [14] studied the pitch and yaw effects on the power output of a fluttering piezoelectric energy harvester. Zakaria [15] et al. developed an energy harvester that harvests energy from self-induced flutter of a composite beam. Bibo and Daqaq [16] provided a single-vibration energy harvester integrated with an airfoil to harvest energy from ambient vibrations and wind. They found that using a single piezoelectric energy harvester under combined aerodynamic loading and ambient vibrations can significantly improve its transduction capability and the overall power density. Wu et al. provided a wind energy harvester comprised of a cantilever attached to piezoelectric patches and a proof mass [17]. Tao et al. developed an energy harvesting device with consideration of a wind turbine and piezoelectric effect [18].

Harvesting wind energy by exploiting vortex-induced vibration (VIV) is another useful way, and has also gained a lot of attention from scientists. Sivadas and Wickenheiser [19] proposed a wind energy harvesting device with a bluff body attached to the trailing edge of a flexible piezoelectric cantilever. Different bluff-body shapes (cylindrical, triangular, and pentagonal) and dimensions are discussed, and the results showed that the bluff body with cylindrical shape can obtain higher average power than the other two bluff-body shapes. Gao et al. [20] found that turbulence excitation was the dominant driving mechanism of the piezoelectric flow energy harvester. Based on the EulerLagrange principle and the Galerkin discretization, Dai et al. [21,22] established the nonlinear distributed-parameter model for harvesting energy from the combination of vibratory base excitations and vortex-induced vibration. Naseer et al. [23] investigated the transduction of piezomagnetoelastic energy harvesting from vortex-induced vibration by introducing nonlinear attractive magnetic forces. Akaydin et al. [24,25] evaluated the performance of energy generators that harvest energy from unsteady and turbulent fluid flow by using piezoelectric cantilever beam.

Harvesting wind energy by exploiting the galloping induced by wind, Zhao et al. [26] studied the effect of tip body on the performance of the piezoelectric energy harvester, and recommended that the tip of square section should be used for galloping energy harvesters. Ewere et al. [27] considered a galloping piezoelectric energy harvester (GPEH) with a rectangular and square prism as the tip bluff body, respectively. Moreover, they proposed an improved GPEH by introducing a bump stop [28]. Sirohi and Mahadik [29] developed a galloping piezoelectric beam with a D-shaped cross-sectional tip body. For the wind energy harvesting device, an approximated distributed-parameter model was used to predict dynamic response and power output of wind energy harvesting devices. For example, Abdelkefi et al. [30] developed a coupled nonlinear distributedparameter model to determine the effects of the cross-sectional geometry, load resistance and wind speed on the level of the harvester power. Zhao et al. [31] proposed a 2-degree-of freedom (2DOF) piezoelectric aeroelastic energy harvester with a cut-out cantilever and two magnets. Hu et al. [32] found that attaching fins to the leading edge significantly improves the efficiency of the harvester. Furthermore, some works about the mechanical response of piezoelectric energy harvesters under combined galloping and base excitations [3335] are also reported.

To reduce the cost of piezoelectric wind energy harvesters, the shape of the cantilever beam should be optimized. However, works about the effect of shape of the cantilever beam on the energy harvesting performance have not been reported so far. In this paper, a nonlinear distribution parameter model for galloping-based piezoelectric energy harvesters with different geometries will be developed. The optimized shape of the cantilever beam will be given.

newpage

Power harvesting refers to energy retraction from ambient surroundingsand convertingitintouseful electric energy. With advances in wireless technology and low-power electronics, energy harvesting from environmental resources has the potential to power mobile and wireless microsystems where battery replacement is either practically impossible or prohibitively expensive [7, 26, 31, 48]. Due to the ubiquitous presence of ambient vibrations, extensive research efforts have been made for converting mechanical energy into electrical power through piezoelectric, electromagnetic and capacitive transducers [36, 40]. Amongst them, piezoelectric vibration-to-electricity converters have been viewed as being superior to other means, as they have high electromechanical coupling, no external voltage source requirement and they are particularly attractive for use in MEMS [15, 20, 40] and nanosystems [28, 38]. As a result, the use of piezoelectric materials for scavenging energy from ambient vibration sources has recently witnessed a dramatic rise for power harvesting [5, 13, 24, 25, 49, 56].

A vibration-based piezoelectric energy harvesting system includes three essential components: an oscillator, a piezoelectric medium and an energy storage circuit, as demonstrated in figure 1. An oscillator is designed to transmit ambient vibrations into mechanical strain energy which is converted into electrical energy via the direct piezoelectric effect. The generated charges are accumulated through an interfacing circuit for AC/DC conversion and presented to a load circuit. Precisely, the power generator is typically designed as a resonant oscillator since the peak power is achieved when the driving frequency matches the devices resonance [40]. The transducermaterialsfor energyconversion include PZT, PVDF and the newly emerged ferroelectric relaxors such as PMN-PT [30, 50]. They have been used in various types of structures to serve specific purposes, such as cantilever beams in transverse excitation bases [1, 16, 35] and plates (diaphragms) in pressure-loaded environments [17, 32]. The layout of electrodes on the plates surfaces has to be carefully patterned to avoid charge cancellation [18, 41]. The designofgenerators based onnon-resonantexcitationshasalso received considerable recent attention [3, 37, 42, 52].

The circuit design is required for electrical compatibility and maximum power transfer to the load. It consists of AC/DC interfacing electronics connecting the piezoelectric element to the terminal electric load. Power optimization schemes therefore depend not only on the mechanical solicitation, but also on the specific types of interfacing circuits. This motivates a variety of research efforts for proposingappropriate electronic interfaces. The mostcommon one is the standard interface which includes an AC/DC rectifier followed by a filtering capacitance, as shown in the middle of figure 1. Ottman et al [33] have studied the electrical behavior of thisstandard system based on the uncoupled model which simplifies the vibrating piezoelectric structure as the current source in parallel with its internal capacitance. They further developed adaptive DC/DC converters for impedance matching [34]. Shu and Lien [44] subsequently proposed an improved analysis for optimizing AC/DC power extraction without the uncoupled assumption. They also investigated the relation between electrically induced damping and conversion efficiency for a rectified piezoelectric device [45] (cf [22, 23, 39]). The result shows that optimization criteria vary according to the relative strength of electromechanical coupling to mechanical damping ratio. Guan and Liao [10, 11] analyzed the charge/discharge efficiencies for several different energy storage devices. Wu et al [54] and Wickenheiser et al [53] investigated the transient behavior of a storage capacitor under charging. Liu et al [27] used the switch-mode power electronics to develop a scheme for active energy harvesting. Basedonthebeam model,Huetal[14]numericallystudiedthe interaction between the piezoelectric vibrating structure and the storage circuit.

Another recently emerged energy harvesting circuit is the synchronized switch harvesting on inductor (SSHI) interface which is added to the piezoelectric element together with the standard DC technique, as also illustrated in the middle of figure 1. This technique was proposed by Guyomar and his co-workers [2, 12, 19, 21, 29] who have shown that power is boosted significantly in a weakly coupled electromechanical system. However, the effect of frequency deviation from resonance on the electrical behavior of an SSHI system is not taken into account in the original analysis. Instead, Shu et al [46] have proposed several improved estimates for the parallel- SSHI circuit accounting for this effect. They have shown that the electrical response of a parallel-SSHI system is similar to that of a strongly coupled electromechanical standard system operated at the short circuit resonance. Furthermore, this technique improves the scavengers bandwidth significantly in comparison to the standard technique. Here, we provide another improved analysis for electrical performance evaluation of a series-SSHI system. It takes into account the full electromechanical coupling response and vibration phase- shift effect, and therefore the analysis is capable of revealing the system characteristics in the vicinity of resonance. The results show that the electrical behaviors of these two ideal SSHI systems are conjugate with each other in comparison to the standard technique.

However, they exhibit a dissimilar responseiftheeffect ofdiodelossisconsidered. Itturnsoutthe feature of wideband could be lost in practical devices endowed with series-SSHI circuits. Finally, some of our preliminary results have been reported in a conference paper [47]. Here, we systematically derive the main results with numerical validation and provide discussions concerning electrical loss in detail.

This paper is organized as follows. First a piezoelectric transducer is modeled as a lumped single-degree-of-freedom system undergoing periodic forcing in section 2. A number of research efforts based on the distributed parameter methods have been made for analyzing a vibrating piezoelectric structure connected to a single resistor [4, 8, 9, 16, 43]. They show advantages in predicting the model shapes, strain distribution and energy harvesting performance based on geometry and material properties of a structure. However, difficulties arise if the nonlinear interfacing circuits are taken into account in analysis [14]. Limited success has been achieved by bridging structural modeling and circuit simulation such as coupled FEMSPICE models [6, 55]. Hence, if the focus is the overall electrical behavior rather than the detailed response at each specific point of a structure, the reduced model suffices the need for harvesting circuit design. Subsequently, an energy harvester using the standard circuit is introduced in section 2.1 and the electrical response of a series-SSHI system is analyzed in detail in section 2.2. The harvested power is derived and expressed explicitly in terms of several dimensionlesssystem parameters. The operating points for achieving optimal power is also discussed there. For the purpose of comparison, the electrical behavior of a parallel-SSHI systemisbrieflyreviewed insection2.3. Next, theresults are numerically validated in section 3.1 and are discussed under the case of non-ideal voltage inversion in section 3.2 and the case of diode loss in section 3.3. The conclusions are made in section 4.

3 Summary of the interested equations

The dynamic equations for a typical piezoelectric composite cantilever beam is

$$B_p \frac{\partial^4 w(x,t)}{\partial x^4} + m_p \frac{\partial^2 w(x,t)}{\partial t^2} = 0, \tag{1}$$

where B_p is the equivalent bending stiffness and m_p is the line mass density of the piezoelectric cantilever beam. If the piezoelectric elements attached to the cantilever beam is connected to an external electrical load R_l, we have

$$\frac{dQ_p(t)}{dt} + \frac{V_p(t)}{R_l} = 0. \tag{2}$$

For the underlying physics, we have the following constitutive equations

$$\begin{aligned} M_p(x,t) &= B_p \frac{\partial^2 w(x,t)}{\partial x^2} - e_p V_p(t), \\ q_p(x,t) &= e_p \frac{\partial^2 w(x,t)}{\partial x^2} + \varepsilon_p V_p(t), \end{aligned} \tag{3}$$

or equivalently,

$$\begin{cases} M_p(x,t) = B_p \dfrac{\partial^2 w(x,t)}{\partial x^2} - e_p V_p(t), \\ Q_p(x,t) = e_p \left[\dfrac{\partial w(x,t)}{\partial x} \right] \Big|_0^{l_p} + C_p V_p(t). \end{cases} \tag{4}$$

One end of the cantilever beam is fixed while the other end is free. So the boundary conditions are

$$\begin{cases} w(0,t) = w_b(t), \\ \dfrac{\partial w(0,t)}{\partial x} = 0, \end{cases} \tag{5}$$

and

$$\begin{cases} M_p(l_p,t) = B_p \dfrac{\partial^2 w(l_p,t)}{\partial x^2} - e_p V_p(t) = 0, \\ N_p(l_p,t) = \dfrac{\partial M_p(l_p,t)}{\partial x} = B_p \dfrac{\partial^3 w(l_p,t)}{\partial x^3} = 0. \end{cases} \tag{6}$$

4 Theoretical solution to the problem

In the classical energy harvesting applications, the cantilever beam is subject to a periodical base excitation $w_b(t)$. Thus the dynamic response of the cantilever beam is decomposed as

$$w(x,t) = w_b(t) + w_{rel}(x,t), \tag{7}$$

where $w_{rel}(x,t)$ is the relative displacement function of the cantilever beam. In this way, the system is converted into

$$B_p \frac{\partial^4 w_{rel}(x,t)}{\partial x^4} + m_p \frac{\partial^2 w_{rel}(x,t)}{\partial t^2} = -m_p \frac{\partial^2 w_b(t)}{\partial t^2}, \tag{8}$$

$$e_p \left[\frac{\partial^2 w_{rel}(x,t)}{\partial x \partial t}\right]\Big|_0^{l_p} + C_p \frac{dV_p(t)}{dt} + \frac{V_p(t)}{R_l} = 0. \tag{9}$$

$$\begin{cases} w_{rel}(0,t) = 0, \\ \dfrac{\partial w_{rel}(0,t)}{\partial x} = 0, \end{cases} \tag{10}$$

and

$$\begin{cases} B_p \dfrac{\partial^2 w_{rel}(l_p,t)}{\partial x^2} - e_p V_p(t) = 0, \\ \dfrac{\partial^3 w_{rel}(l_p,t)}{\partial x^3} = 0. \end{cases} \tag{11}$$

Considering a sinusoidal base excitation

$$w_b(t) = \eta_b e^{j\sigma_b t} \tag{12}$$

where ξ_b is usually a real vibration amplitude, the steady state solution for the above system can be reasonably set as

$$w_{rel}(x,t) = \eta_{rel}(x) e^{j\sigma_b t}, \quad V_p(t) = \tilde{V}_p e^{j\sigma_b t}, \tag{13}$$

where $\eta_{rel}(x)$ and $\tilde{V}_p$ are complex amplitudes. Then the above system is again simplified as

$$B_p \frac{\partial^4 \eta_{rel}(x)}{\partial x^4} - m_p \sigma_b^2 \eta_{rel}(x) = m_p \sigma_b^2 \eta_b, \tag{14}$$

$$\begin{cases} \eta_{rel}(0) = 0, \\ \dfrac{\partial \eta_{rel}(0)}{\partial x} = 0, \end{cases} \tag{15}$$

and

$$\begin{cases} B_p \dfrac{\partial^2 \eta_{rel}(l_p)}{\partial x^2} + \dfrac{j\sigma_b R_l}{1 + j\sigma_b C_p R_l} e_p^2 \dfrac{\partial \eta_{rel}(l_p)}{\partial x} = 0, \\ \dfrac{\partial^3 \eta_{rel}(l_p)}{\partial x^3} = 0. \end{cases} \tag{16}$$

Note that here we assume a sinusoidal steady state response, which is not actually validated theoretically.

Obviously we can have the following dimensionless scheme:

$$\eta_{rel} \sim u\eta_b, \quad x \sim z l_p \tag{17}$$

and therefore the following dimensionless parameters

$$\sigma = \sigma_b \sqrt{\frac{m_p l_p^4}{B_p}}, \quad \beta = R_l C_p \sqrt{\frac{B_p}{m_p l_p^4}}, \quad \delta = \frac{e_p^2 l_p}{C_p B_p}. \tag{18}$$

Now, we reach the following dimensionless system of boundary value problem

$$\begin{cases} u'''' - \sigma^2 u = \sigma^2, \\ u(0) = 0, \\ u'(0) = 0, \\ u''(1) + \dfrac{j\beta\sigma}{1 + j\beta\sigma} \delta u'(1) = 0, \\ u'''(1) = 0, \end{cases} \tag{19}$$

where the prime denotes the derivative with respect to z. The analytical solution to this problem can be formulated as

$$u(z;\delta) = A_\delta \cos\sqrt{\sigma}z + B_\delta \sin\sqrt{\sigma}z + C_\delta \cosh\sqrt{\sigma}z + D_\delta \sinh\sqrt{\sigma}z - 1 \tag{20}$$

and hence

$$\begin{aligned} u'(z;\delta) &= \sigma^{1/2}\left(-A_\delta \sin\sqrt{\sigma}z + B_\delta \cos\sqrt{\sigma}z + C_\delta \sinh\sqrt{\sigma}z + D_\delta \cosh\sqrt{\sigma}z\right), \\ u''(z;\delta) &= \sigma\left(-A_\delta \cos\sqrt{\sigma}z - B_\delta \sin\sqrt{\sigma}z + C_\delta \cosh\sqrt{\sigma}z + D_\delta \sinh\sqrt{\sigma}z\right), \\ u'''(z;\delta) &= \sigma^{3/2}\left(A_\delta \sin\sqrt{\sigma}z - B_\delta \cos\sqrt{\sigma}z + C_\delta \sinh\sqrt{\sigma}z + D_\delta \cosh\sqrt{\sigma}z\right). \end{aligned} \tag{21}$$

The coefficients A_δ, B_δ, C_δ, and D_δ are then subject to the following linear system of equations:

$$\begin{cases} A_\delta + C_\delta = 1, \\ B_\delta + D_\delta = 0, \\ \left(-A_\delta \cos\sqrt{\sigma} - B_\delta \sin\sqrt{\sigma} + C_\delta \cosh\sqrt{\sigma} + D_\delta \sinh\sqrt{\sigma}\right) + \\ \dfrac{j\beta\sqrt{\sigma}}{j\sigma\beta+1}\delta\left(-A_\delta \sin\sqrt{\sigma} + B_\delta \cos\sqrt{\sigma} + C_\delta \sinh\sqrt{\sigma} + D_\delta \cosh\sqrt{\sigma}\right) = 0, \\ A_\delta \sin\sqrt{\sigma} - B_\delta \cos\sqrt{\sigma} + C_\delta \sinh\sqrt{\sigma} + D_\delta \cosh\sqrt{\sigma} = 0. \end{cases} \tag{22}$$

Analytically, we can directly obtain the solution to this problem as

$$\begin{cases} A_\delta = \dfrac{1 + \cos\sqrt{\sigma}\cosh\sqrt{\sigma} - \sin\sqrt{\sigma}\sinh\sqrt{\sigma} + \frac{2j\beta\sqrt{\sigma}}{1+j\beta\sigma}\delta\left(\cos\sqrt{\sigma}\sinh\sqrt{\sigma}\right)}{2\left[1 + \cos\sqrt{\sigma}\cosh\sqrt{\sigma} + \frac{j\beta\sqrt{\sigma}}{1+j\beta\sigma}\delta\left(\cos\sqrt{\sigma}\sinh\sqrt{\sigma} + \sin\sqrt{\sigma}\cosh\sqrt{\sigma}\right)\right]}, \\ B_\delta = \dfrac{\cos\sqrt{\sigma}\sinh\sqrt{\sigma} + \sin\sqrt{\sigma}\cosh\sqrt{\sigma} + \frac{2j\beta\sqrt{\sigma}}{1+j\beta\sigma}\delta\left(\sin\sqrt{\sigma}\sinh\sqrt{\sigma}\right)}{2\left[1 + \cos\sqrt{\sigma}\cosh\sqrt{\sigma} + \frac{j\beta\sqrt{\sigma}}{1+j\beta\sigma}\delta\left(\cos\sqrt{\sigma}\sinh\sqrt{\sigma} + \sin\sqrt{\sigma}\cosh\sqrt{\sigma}\right)\right]}, \\ C_\delta = \dfrac{1 + \cos\sqrt{\sigma}\cosh\sqrt{\sigma} + \sin\sqrt{\sigma}\sinh\sqrt{\sigma} + \frac{2j\beta\sqrt{\sigma}}{1+j\beta\sigma}\delta\left(\sin\sqrt{\sigma}\cosh\sqrt{\sigma}\right)}{2\left[1 + \cos\sqrt{\sigma}\cosh\sqrt{\sigma} + \frac{j\beta\sqrt{\sigma}}{1+j\beta\sigma}\delta\left(\cos\sqrt{\sigma}\sinh\sqrt{\sigma} + \sin\sqrt{\sigma}\cosh\sqrt{\sigma}\right)\right]}, \\ D_\delta = \dfrac{-\cos\sqrt{\sigma}\sinh\sqrt{\sigma} - \sin\sqrt{\sigma}\cosh\sqrt{\sigma} - \frac{2j\beta\sqrt{\sigma}}{1+j\beta\sigma}\delta\left(\sin\sqrt{\sigma}\sinh\sqrt{\sigma}\right)}{2\left[1 + \cos\sqrt{\sigma}\cosh\sqrt{\sigma} + \frac{j\beta\sqrt{\sigma}}{1+j\beta\sigma}\delta\left(\cos\sqrt{\sigma}\sinh\sqrt{\sigma} + \sin\sqrt{\sigma}\cosh\sqrt{\sigma}\right)\right]}. \end{cases} \tag{23}$$

Firstly, to validate the closed form solution $u(z;\delta)$, we calcaulate the corresponding normalized output voltage $|\tilde{V}_p/(\sigma_b^2\xi_b)|$ and plot the results with respect to the base excitation frequency fr at different externally connected resistance R_l. The results are shown in Figure 1. According to the results, our calculations show a good agreement with those presented in the reference. [9]. Thus we have validated the model and the results and made our preparations for future analysis. It should be noted that, out results show an obvious difference from those in the literature [9] near the resonant frequencies. This could explained as follows. In our numerical calculations, the frequency range can be chosen to be as small as possible. A finer calculation grid leads to a sharper resonant peak. Another point to be noted is that at the resonant peak, the output voltage should arrive at its maximum and its derivative with resepct to fr should be zero and the second order derivative should be infinity. In this way, a small discrpency of the frequency from the resonant frequency leads to a large change in the normalized output voltage.

Secondly, according to equations (20) and (23), the dimensionless displacement amplitude function $u(z)$ is totally determined by the three dimensionless parameters σ, β, and δ introduced before. Among the dimensionless parameters, σ is the dimensionless base excitation frequency, β is the dimensionless electrical resonant frequency, and δ is the dimensionless electromechanical coupling strength for the structure. As σ and β is determined by the base excitation and externally connected circuit respectively, only the parameter δ is fully determined by the structure itself. Hence we would like to investigate the influence of parameter δ upon the solution displacement function $u(z)$. By taking different values of δ , we calculate the displacement amplitude function $u(z)$ and plot the results in Figure 2.

It is shown in Figure 2, the parameter δ changes the function $u(z)$ through the change of the third boundary condition (to be inserted). When δ is zero, i.e., no electromechanical coupling is

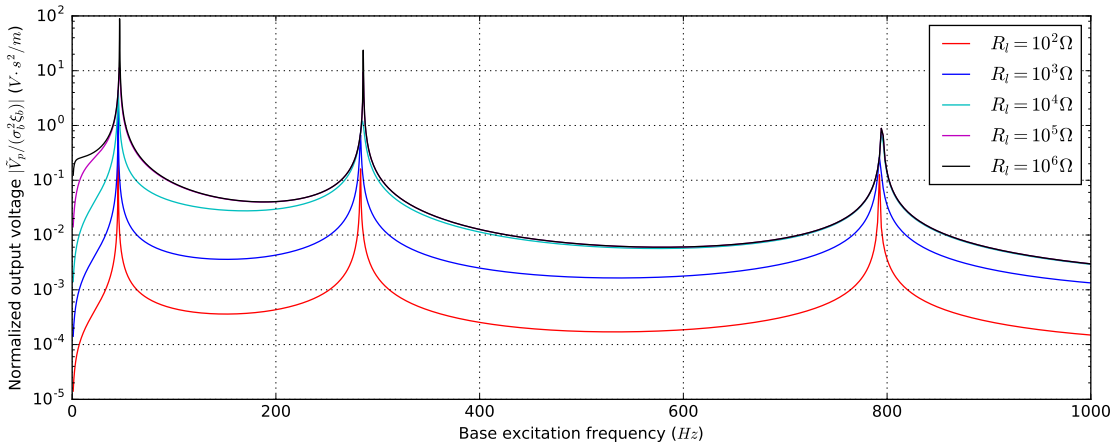

Figure 1: Validation calculation of the normalized output voltage versus base excitation frequency for a unimorph piezoelectric cantilever energy harvester based on the data from [9].

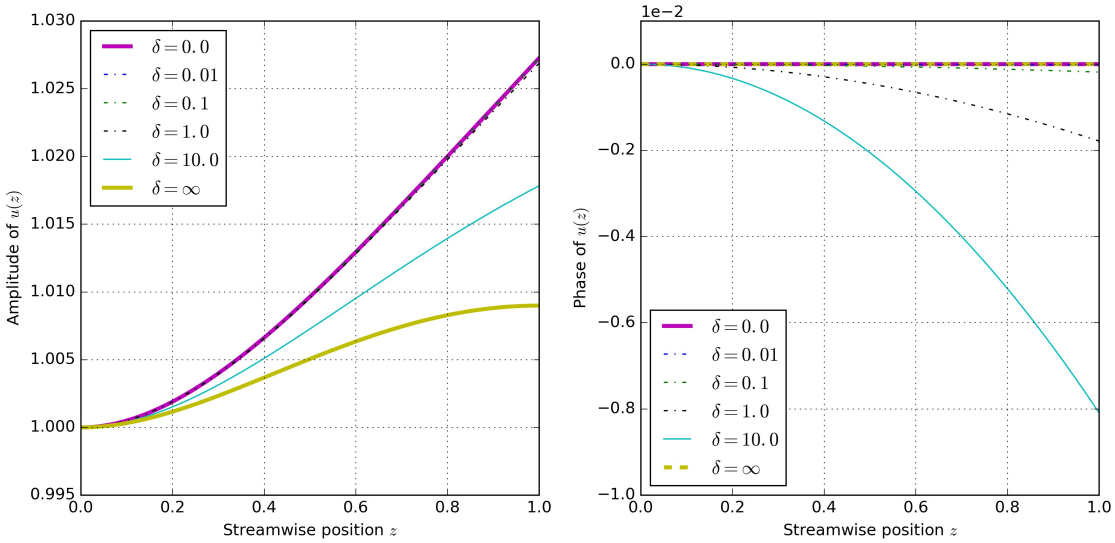

Figure 2: Amplitude and phase of the displacement function $u(z)$ for difference values of δ

present, the system degenerates to the classical elastic cantilever beam problem, whose solution is a real function. That is to say, the phase of $u(z)$ is a constant across the whole beam (in the range of $0 \leq z \leq 1$). Analytical expressions for the coefficients are

$$\begin{cases} A_{\varnothing} = \dfrac{1 + \cos\sqrt{\sigma}\cosh\sqrt{\sigma} - \sin\sqrt{\sigma}\sinh\sqrt{\sigma}}{2\left[1 + \cos\sqrt{\sigma}\cosh\sqrt{\sigma}\right]}, \\ B_{\varnothing} = \dfrac{\cos\sqrt{\sigma}\sinh\sqrt{\sigma} + \sin\sqrt{\sigma}\cosh\sqrt{\sigma}}{2\left[1 + \cos\sqrt{\sigma}\cosh\sqrt{\sigma}\right]}, \\ C_{\varnothing} = \dfrac{1 + \cos\sqrt{\sigma}\cosh\sqrt{\sigma} + \sin\sqrt{\sigma}\sinh\sqrt{\sigma}}{2\left[1 + \cos\sqrt{\sigma}\cosh\sqrt{\sigma}\right]}, \\ D_{\varnothing} = \dfrac{-\cos\sqrt{\sigma}\sinh\sqrt{\sigma} - \sin\sqrt{\sigma}\cosh\sqrt{\sigma}}{2\left[1 + \cos\sqrt{\sigma}\cosh\sqrt{\sigma}\right]}. \end{cases} \tag{24}$$

and the resulting dimensionless displacement function $u_{\varnothing}(z)$ is represented as

$$u_{\varnothing}(z) = A_{\varnothing}\cos\sqrt{\sigma}z + B_{\varnothing}\sin\sqrt{\sigma}z + C_{\varnothing}\cosh\sqrt{\sigma}z + D_{\varnothing}\sinh\sqrt{\sigma}z - 1. \tag{25}$$

When the electromechanical coupling is extremely strong, and δ is extremely large and can be seen as ∞ in mathematical sense. In this situation, the solution $u_{\infty}(z)$ is again real without any phase difference in the z direction. The coefficients can be analytically expressed as

$$\begin{cases} A_{\infty} = \dfrac{\cos\sqrt{\sigma}\sinh\sqrt{\sigma}}{\cos\sqrt{\sigma}\sinh\sqrt{\sigma} + \sin\sqrt{\sigma}\cosh\sqrt{\sigma}}, \\ B_{\infty} = \dfrac{\sin\sqrt{\sigma}\sinh\sqrt{\sigma}}{\cos\sqrt{\sigma}\sinh\sqrt{\sigma} + \sin\sqrt{\sigma}\cosh\sqrt{\sigma}}, \\ C_{\infty} = \dfrac{\sin\sqrt{\sigma}\cosh\sqrt{\sigma}}{\cos\sqrt{\sigma}\sinh\sqrt{\sigma} + \sin\sqrt{\sigma}\cosh\sqrt{\sigma}}, \\ D_{\infty} = \dfrac{-\sin\sqrt{\sigma}\sinh\sqrt{\sigma}}{\cos\sqrt{\sigma}\sinh\sqrt{\sigma} + \sin\sqrt{\sigma}\cosh\sqrt{\sigma}}. \end{cases} \tag{26}$$

and hence the dimensionless displacement function $u_{\infty}(z)$ is

$$u_{\infty}(z) = A_{\infty}\cos\sqrt{\sigma}z + B_{\infty}\sin\sqrt{\sigma}z + C_{\infty}\cosh\sqrt{\sigma}z + D_{\infty}\sinh\sqrt{\sigma}z - 1. \tag{27}$$

While a finite non-zero electromechanical coupling factor δ is present, which is expected in most applications, the resulting dimensionless displacement function $u(z)$ has varying magnitude and phase along the stream-wise direction or z direction. Nevertheless, it is seen from the right panel of Figure 2 that for different values of δ, the phase change of $u(z)$ is very small in the z direction, actually in the order 10^{-2}.

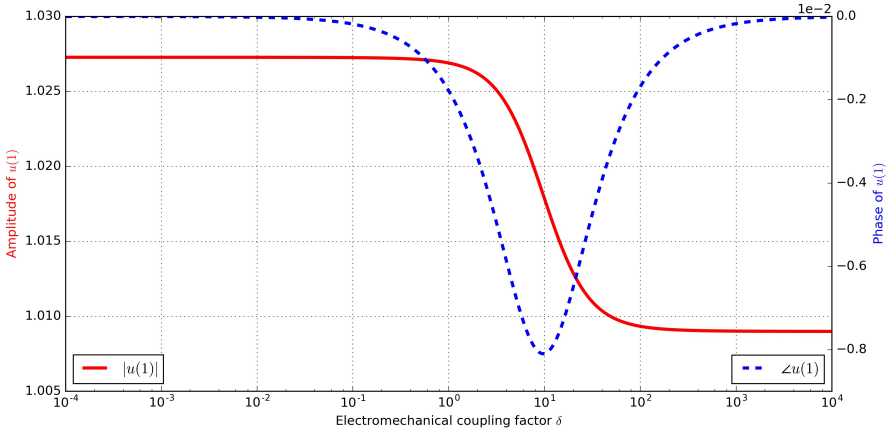

Figure 3: Amplitude and phase of the displacement function $u(z)$ at the position $z = 1$ versus electromechanical coupling factor δ.

To make it more clear, we plot the phase of $u(z)$ at $z = 1$ versus different values of δ in Figure 3. It is clear that with the increase of δ, amplitude of the end displamcent ($z = 1$) of the beam

$|u(z)|$ decreases, while its phase reaches a minimum at around $\delta = 10$. This also explains the fact expressed in Figure 2 that the amplitude of displacement function $u_\delta(z)$ with $0 < \delta < \infty$ is always between that of $u_\varnothing(z)$ and $u_\infty(z)$.

As for the output voltage $V_p(t)$, output current $I_p(t)$, and output power $P_p(t)$ for the classical piezoelectric cantilever energy harvester, their corresponding complex amplitudes $\tilde{V}_p$, $\tilde{I}_p$, and $\tilde{P}_p$ can be formulated as

$$\begin{cases} \tilde{V}_p = -\dfrac{j\sigma\beta}{j\sigma\beta+1}\dfrac{\eta_b}{l_p}\dfrac{e_p}{C_p}u'(1), \\ \quad = -\dfrac{j\sigma\beta}{j\sigma\beta+1}\dfrac{\eta_b}{l_p}\dfrac{e_p}{C_p}\sigma^{1/2}\left(-A_\delta\sin\sqrt{\sigma}+B_\delta\cos\sqrt{\sigma}+C_\delta\sinh\sqrt{\sigma}+D_\delta\cosh\sqrt{\sigma}\right) \\ \quad = -\dfrac{j\sigma\beta}{j\sigma\beta+1}\dfrac{\eta_b}{l_p}\dfrac{e_p}{C_p}\dfrac{\sqrt{\sigma}\left(\sinh\sqrt{\sigma}-\sin\sqrt{\sigma}\right)}{1+\cos\sqrt{\sigma}\cosh\sqrt{\sigma}+\frac{j\beta\sqrt{\sigma}}{1+j\beta\sigma}\delta\left(\cos\sqrt{\sigma}\sinh\sqrt{\sigma}+\sin\sqrt{\sigma}\cosh\sqrt{\sigma}\right)} \\ \quad = -\dfrac{j\sigma\beta}{j\sigma\beta+1}\left(\dfrac{\eta_b}{l_p}\right)\left(\dfrac{e_p}{C_p}\right)\chi_p, \\ \tilde{I}_p = \tilde{V}_p/R_l = -\dfrac{j\sigma\beta}{j\sigma\beta+1}\left(\dfrac{\eta_b}{l_p}\right)\left(\dfrac{e_p}{C_pR_l}\right)\chi_p, \\ \tilde{P}_p = \tilde{V}_p^2/R_l = \left(\dfrac{\eta_b}{l_p}\right)^2\left(\dfrac{e_p}{C_p}\right)\left(\dfrac{e_p}{C_pR_l}\right)\left(\dfrac{j\sigma\beta}{j\sigma\beta+1}\right)^2\chi_p^2, \end{cases} \tag{28}$$

in which we have used the notations that

$$\chi_p = u_1'(1) = \frac{\sqrt{\sigma}\left(\sinh\sqrt{\sigma}-\sin\sqrt{\sigma}\right)}{1+\cos\sqrt{\sigma}\cosh\sqrt{\sigma}+\frac{j\beta\sqrt{\sigma}}{1+j\beta\sigma}\delta\left(\cos\sqrt{\sigma}\sinh\sqrt{\sigma}+\sin\sqrt{\sigma}\cosh\sqrt{\sigma}\right)}. \tag{29}$$

Clearly, The three output measures $\tilde{V}_p$, $\tilde{I}_p$, and $\tilde{P}_p$ are heavily dependent on another dimensionless parameter $r_d = \eta_b/l_p$. Formally, both $\tilde{V}_p$ and $\tilde{I}_p$ depend lineary upon r_d, while $\tilde{P}_p$ shows a quadratic dependence on r_d. The only dependence upon δ is introduced in χ_p. However, it should be noted that the parameter δ relies on e_p, l_p, C_p, and B_p, while the three measures $\tilde{V}_p$, $\tilde{I}_p$, and $\tilde{P}_p$ are dimensional values and depend on e_p, σ_b, and R_l. As a result, the change of parameter δ results in the change of reference voltage e_p/C_p, reference current $e_p/(C_pR_l)$, and reference power $(e_p/C_p)[e_p/(C_pR_l)]$, and therefore the corresponding values of $\tilde{V}_p$, $\tilde{I}_p$, and $\tilde{P}_p$. Hence, we may establish a bijective relation between δ and e_p, and relate the change of δ to that of e_p. In this way, we calculate the output measures at different values of δ and plot their amplitudes in Figure 4.

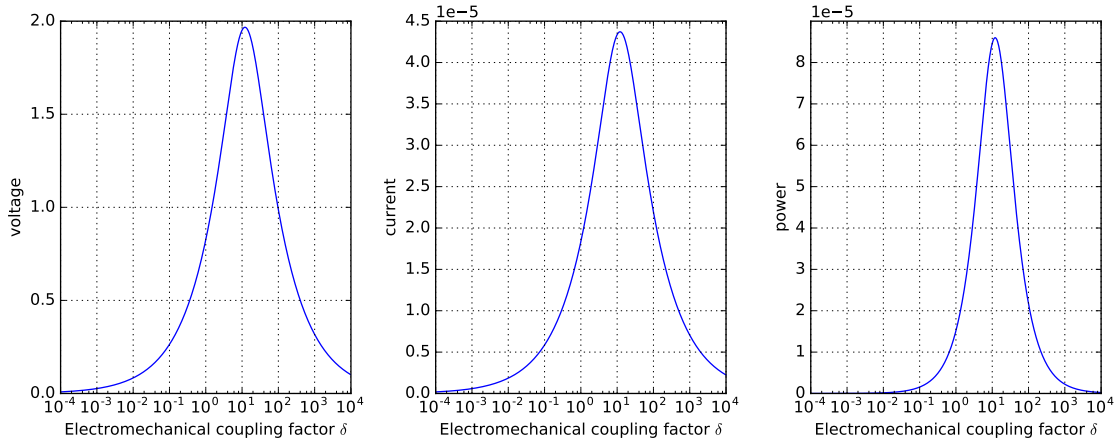

Figure 4: Voltage, current and power output for the piezoelectric cantilever energy harvester

It is seen from Figure 4 that all the three measures show a maximum peak with the increase of δ at the approximate value of $\delta = 10$. When δ is small, or equivalently, e_p is small, amplitude of the three output measures $\tilde{V}_p$, $\tilde{I}_p$, and $\tilde{P}_p$ increase with the increase of δ. Then after the critical value of δ, a further increase of δ causes the decrease of output measures. Thus we come to a small conclusion

that to obtain an optimal output performance, the electromechanical coupling factor δ should be set to an appropriate value. However, a direct calculation using the parameters introduced in the literature [9, 10] shows that the parameter δ is rather small for a typical piezoelectric cantilever energy harvester. For example, for a piezoelectric voltage constant $e_{31} = -5.35\ C/m^2$, the value of e_p is $-5.35 \times 10^{-5}\ C$, and the final value of δ is 0.028. According to the properties of commonly used piezoelectric materials, the parameter e_{31} is always in the range of several or several tens C/m^2 reference to be inserted. That is to say, the final value of δ can be seen always in the order of 10^{-2}, which is a rather small value according to the diagram. Hence we could present an asymptotic analysis of the performance of the classical piezoelectric energy harvester. This is the subject of the following section.

5 Asymptotic analysis of the problem

Considering that the parameter δ is small, we expand the theoretical solution to the problem in terms of the small parameter δ using the following regular expansion:

$$\begin{cases} A_\delta = A_0 + \delta A_1 + \delta^2 A_2 + \cdots, \\ B_\delta = B_0 + \delta B_1 + \delta^2 B_2 + \cdots, \\ C_\delta = C_0 + \delta C_1 + \delta^2 C_2 + \cdots, \\ D_\delta = D_0 + \delta D_1 + \delta^2 D_2 + \cdots. \end{cases} \tag{30}$$

As a result, we obtain the following successive expansion problem:
$O(\delta^0)$:

$$\begin{cases} A_0 + C_0 = 1, \\ B_0 + D_0 = 0, \\ -A_0 \cos\sqrt{\sigma} - B_0 \sin\sqrt{\sigma} + C_0 \cosh\sqrt{\sigma} + D_0 \sinh\sqrt{\sigma} = 0, \\ A_0 \sin\sqrt{\sigma} - B_0 \cos\sqrt{\sigma} + C_0 \sinh\sqrt{\sigma} + D_0 \cosh\sqrt{\sigma} = 0. \end{cases} \tag{31}$$

The solution is

$$\begin{cases} A_0 = \dfrac{1 + \cos\sqrt{\sigma}\cosh\sqrt{\sigma} - \sin\sqrt{\sigma}\sinh\sqrt{\sigma}}{2 + 2\cos\sqrt{\sigma}\cosh\sqrt{\sigma}}, \\ B_0 = \dfrac{\cosh\sqrt{\sigma}\sin\sqrt{\sigma} + \cos\sqrt{\sigma}\sinh\sqrt{\sigma}}{2 + 2\cos\sqrt{\sigma}\cosh\sqrt{\sigma}}, \\ C_0 = \dfrac{1 + \cos\sqrt{\sigma}\cosh\sqrt{\sigma} + \sin\sqrt{\sigma}\sinh\sqrt{\sigma}}{2 + 2\cos\sqrt{\sigma}\cosh\sqrt{\sigma}}, \\ D_0 = -\dfrac{\cosh\sqrt{\sigma}\sin\sqrt{\sigma} + \cos\sqrt{\sigma}\sinh\sqrt{\sigma}}{2 + 2\cos\sqrt{\sigma}\cosh\sqrt{\sigma}}. \end{cases} \tag{32}$$

Hence we have

$$-A_0 \sin\sqrt{\sigma} + B_0 \cos\sqrt{\sigma} + C_0 \sinh\sqrt{\sigma} + D_0 \cosh\sqrt{\sigma} = \frac{\sinh\sqrt{\sigma} - \sin\sqrt{\sigma}}{\cos\sqrt{\sigma}\cosh\sqrt{\sigma} + 1} \tag{33}$$

$O(\delta^1)$:

$$\begin{cases} A_1 + C_1 = 0, \\ B_1 + D_1 = 0, \\ \dfrac{j\beta\sqrt{\sigma}}{j\sigma\beta + 1}\left(-A_1 \cos\sqrt{\sigma} - B_1 \sin\sqrt{\sigma} + C_1 \cosh\sqrt{\sigma} + D_1 \sinh\sqrt{\sigma}\right) + \\ \qquad \left(-A_0 \sin\sqrt{\sigma} + B_0 \cos\sqrt{\sigma} + C_0 \sinh\sqrt{\sigma} + D_0 \cosh\sqrt{\sigma}\right) = 0, \\ A_1 \sin\sqrt{\sigma} - B_1 \cos\sqrt{\sigma} + C_1 \sinh\sqrt{\sigma} + D_1 \cosh\sqrt{\sigma} = 0. \end{cases} \tag{34}$$

The solution is

$$\begin{cases} A_1 = \dfrac{j\beta\sqrt{\sigma}}{1+j\beta\sigma}\left(\dfrac{\sinh\sqrt{\sigma}-\sin\sqrt{\sigma}}{\cos\sqrt{\sigma}\cosh\sqrt{\sigma}+1}\right)\left(\dfrac{\cos\sqrt{\sigma}+\cosh\sqrt{\sigma}}{2\cos\sqrt{\sigma}\cosh\sqrt{\sigma}+2}\right) \\ B_1 = \dfrac{j\beta\sqrt{\sigma}}{1+j\beta\sigma}\left(\dfrac{\sinh\sqrt{\sigma}-\sin\sqrt{\sigma}}{\cos\sqrt{\sigma}\cosh\sqrt{\sigma}+1}\right)\left(\dfrac{-\sinh\sqrt{\sigma}+\sin\sqrt{\sigma}}{2\cos\sqrt{\sigma}\cosh\sqrt{\sigma}+2}\right) \\ C_1 = \dfrac{j\beta\sqrt{\sigma}}{1+j\beta\sigma}\left(\dfrac{\sinh\sqrt{\sigma}-\sin\sqrt{\sigma}}{\cos\sqrt{\sigma}\cosh\sqrt{\sigma}+1}\right)\left(-\dfrac{\cos\sqrt{\sigma}+\cosh\sqrt{\sigma}}{2\cos\sqrt{\sigma}\cosh\sqrt{\sigma}+2}\right) \\ D_1 = \dfrac{j\beta\sqrt{\sigma}}{1+j\beta\sigma}\left(\dfrac{\sinh\sqrt{\sigma}-\sin\sqrt{\sigma}}{\cos\sqrt{\sigma}\cosh\sqrt{\sigma}+1}\right)\left(\dfrac{-\sin\sqrt{\sigma}+\sinh\sqrt{\sigma}}{2\cos\sqrt{\sigma}\cosh\sqrt{\sigma}+2}\right) \end{cases} \tag{35}$$

Then we have

$$\begin{aligned} &-A_1\sin\sqrt{\sigma}+B_1\cos\sqrt{\sigma}+C_1\sinh\sqrt{\sigma}+D_1\cosh\sqrt{\sigma} \\ &=\frac{j\beta\sqrt{\sigma}}{1+j\beta\sigma}\left(\frac{\sin\sqrt{\sigma}-\sinh\sqrt{\sigma}}{\cos\sqrt{\sigma}\cosh\sqrt{\sigma}+1}\right)\left(\frac{\cos\sqrt{\sigma}\sinh\sqrt{\sigma}+\sin\sqrt{\sigma}\cosh\sqrt{\sigma}}{\cos\sqrt{\sigma}\cosh\sqrt{\sigma}+1}\right) \end{aligned} \tag{36}$$

$O(\delta^2)$:

$$\begin{cases} A_2+C_2=0, \\ B_2+D_2=0, \\ \left(-A_2\cos\sqrt{\sigma}-B_2\sin\sqrt{\sigma}+C_2\cosh\sqrt{\sigma}+D_2\sinh\sqrt{\sigma}\right)+ \\ \dfrac{j\beta\sqrt{\sigma}}{j\sigma\beta+1}\left(-A_1\sin\sqrt{\sigma}+B_1\cos\sqrt{\sigma}+C_1\sinh\sqrt{\sigma}+D_1\cosh\sqrt{\sigma}\right)=0, \\ A_2\sin\sqrt{\sigma}-B_2\cos\sqrt{\sigma}+C_2\sinh\sqrt{\sigma}+D_2\cosh\sqrt{\sigma}=0. \end{cases} \tag{37}$$

The solution is

$$\begin{cases} A_2 = \left(\dfrac{j\beta\sqrt{\sigma}}{1+j\beta\sigma}\right)^2\left(\dfrac{\sinh\sqrt{\sigma}-\sin\sqrt{\sigma}}{\cos\sqrt{\sigma}\cosh\sqrt{\sigma}+1}\right)\left(\dfrac{\cos\sqrt{\sigma}\sinh\sqrt{\sigma}+\sin\sqrt{\sigma}\cosh\sqrt{\sigma}}{\cos\sqrt{\sigma}\cosh\sqrt{\sigma}+1}\right)\left(\dfrac{\cos\sqrt{\sigma}+\cosh\sqrt{\sigma}}{2\cos\sqrt{\sigma}\cosh\sqrt{\sigma}+2}\right) \\ B_2 = \left(\dfrac{j\beta\sqrt{\sigma}}{1+j\beta\sigma}\right)^2\left(\dfrac{\sinh\sqrt{\sigma}-\sin\sqrt{\sigma}}{\cos\sqrt{\sigma}\cosh\sqrt{\sigma}+1}\right)\left(\dfrac{\cos\sqrt{\sigma}\sinh\sqrt{\sigma}+\sin\sqrt{\sigma}\cosh\sqrt{\sigma}}{\cos\sqrt{\sigma}\cosh\sqrt{\sigma}+1}\right)\left(\dfrac{-\sinh\sqrt{\sigma}+\sin\sqrt{\sigma}}{2\cos\sqrt{\sigma}\cosh\sqrt{\sigma}+2}\right) \\ C_2 = \left(\dfrac{j\beta\sqrt{\sigma}}{1+j\beta\sigma}\right)^2\left(\dfrac{\sinh\sqrt{\sigma}-\sin\sqrt{\sigma}}{\cos\sqrt{\sigma}\cosh\sqrt{\sigma}+1}\right)\left(\dfrac{\cos\sqrt{\sigma}\sinh\sqrt{\sigma}+\sin\sqrt{\sigma}\cosh\sqrt{\sigma}}{\cos\sqrt{\sigma}\cosh\sqrt{\sigma}+1}\right)\left(-\dfrac{\cos\sqrt{\sigma}+\cosh\sqrt{\sigma}}{2\cos\sqrt{\sigma}\cosh\sqrt{\sigma}+2}\right) \\ D_2 = \left(\dfrac{j\beta\sqrt{\sigma}}{1+j\beta\sigma}\right)^2\left(\dfrac{\sinh\sqrt{\sigma}-\sin\sqrt{\sigma}}{\cos\sqrt{\sigma}\cosh\sqrt{\sigma}+1}\right)\left(\dfrac{\cos\sqrt{\sigma}\sinh\sqrt{\sigma}+\sin\sqrt{\sigma}\cosh\sqrt{\sigma}}{\cos\sqrt{\sigma}\cosh\sqrt{\sigma}+1}\right)\left(\dfrac{-\sin\sqrt{\sigma}+\sinh\sqrt{\sigma}}{2\cos\sqrt{\sigma}\cosh\sqrt{\sigma}+2}\right) \end{cases} \tag{38}$$

Indeed, we can continue to obtain the coefficients for higher order (≥ 2) expansions, as shown in the appendices (To add some comments) using successive iteration method. Nevertheless, it suffices here to consider up to the second order expansion $u^{(0)}(z)$, $u^{(1)}(z)$, and $u^{(2)}(z)$, respectively:

$$\begin{cases} u^{(0)}(z) = u_0(z), \\ u^{(1)}(z) = u_0(z)+\delta u_1(z), \\ u^{(2)}(z) = u_0(z)+\delta u_1(z)+\delta^2 u_2(z), \end{cases} \tag{39}$$

where the terms $u_0(z)$, $u_1(z)$, and $u_2(z)$ are defined as

$$\begin{cases} u_0(z) = A_0\cos\sqrt{\sigma}z+B_0\sin\sqrt{\sigma}z+C_0\cosh\sqrt{\sigma}z+D_0\sinh\sqrt{\sigma}z-1, \\ u_1(z) = A_1\cos\sqrt{\sigma}z+B_1\sin\sqrt{\sigma}z+C_1\cosh\sqrt{\sigma}z+D_1\sinh\sqrt{\sigma}z, \\ u_2(z) = A_2\cos\sqrt{\sigma}z+B_2\sin\sqrt{\sigma}z+C_2\cosh\sqrt{\sigma}z+D_2\sinh\sqrt{\sigma}z. \end{cases} \tag{40}$$

For different values of δ and σ (Here in this simulation, the value of σ is changed through the variance of base excitation frequency f_b), the asymptotic approximations of the dimensionless relative beam displacement function $u(z;\delta)$ up to the second order $u^{(0)}(z)$, $u^{(1)}(z)$, and $u^{(2)}(z)$ are calculated and compared to the closed solution $u(z;\delta)$ itself. The results are shown in Figure 5, 6, 7, 8, 9, 10, 11.

Notice from Figure 1 that the first mode resonant frequency for the device is around 45 Hz. It is seen from these results that a smaller value of δ results in a better approximation, whatever the value of f_b. This is consistent with the philosophy behind asymptotic expansion. Besides, for the frequency away from the resonant frequency, the approximation results are relatively accurate in the

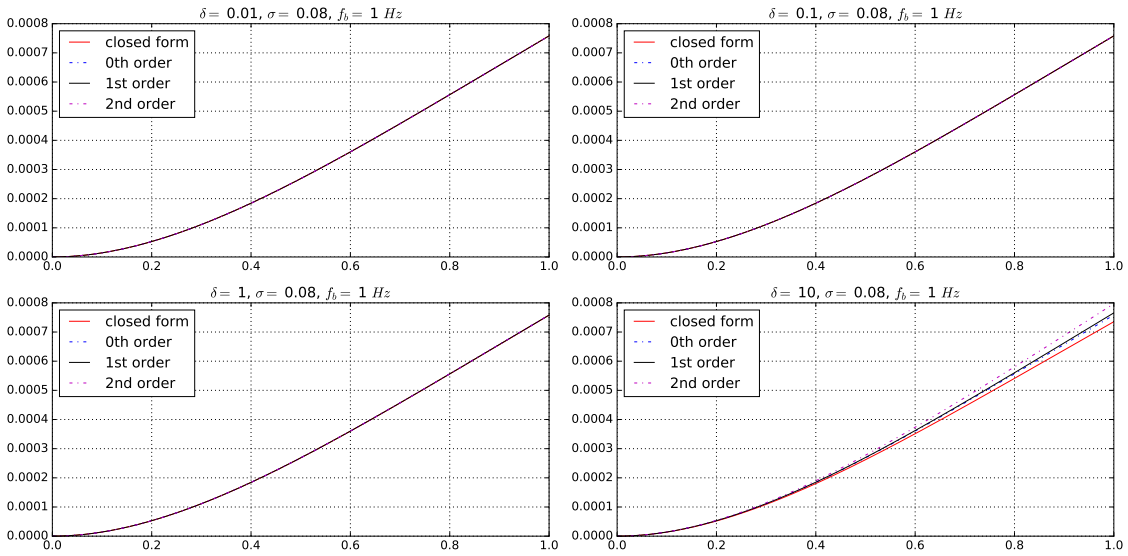

Figure 5: Comparison for the different orders of asymptotic expansion for the dimensionless relative displacement function $u_\delta(z)$.

range of $\delta \leq 0.1$ depending on the value of f_b. While when the base exciation frequency f_b is close to a resonance, for exmaple $f_b = 45\ Hz$, the approximation results are not accurate even at the value of $\delta = 0.01$. That is to say, the asymptotic expansion in terms of δ is not uniform with respect to parameter σ. Especially, the existence of resonance actually restrict the behavior of the asymptotic expansion. Around the resonance the expansion will show low accuracy, while away from the resonance, the expansion accuracy is easily retained. Nonetheless, for commonly used piezoelectric materials and energy harvesting device configuration, the value of δ is usually in the range of 10^{-2}. Hence, it is generally validated to use the asymptotic expansion method to approximate the dimensionless displacement function $u(z;\delta)$. Furtherly, in view of the aprroximating performances of the asymptotic expansions to different orders, it suffices to keep only the $0th$ order terms. Then, we have that

$$u(z;\delta) \approx u^{(0)}(z) = A_0 \cos\sqrt{\sigma}z + B_0 \sin\sqrt{\sigma}z + C_0 \cosh\sqrt{\sigma}z + D_0 \sinh\sqrt{\sigma}z - 1. \tag{41}$$

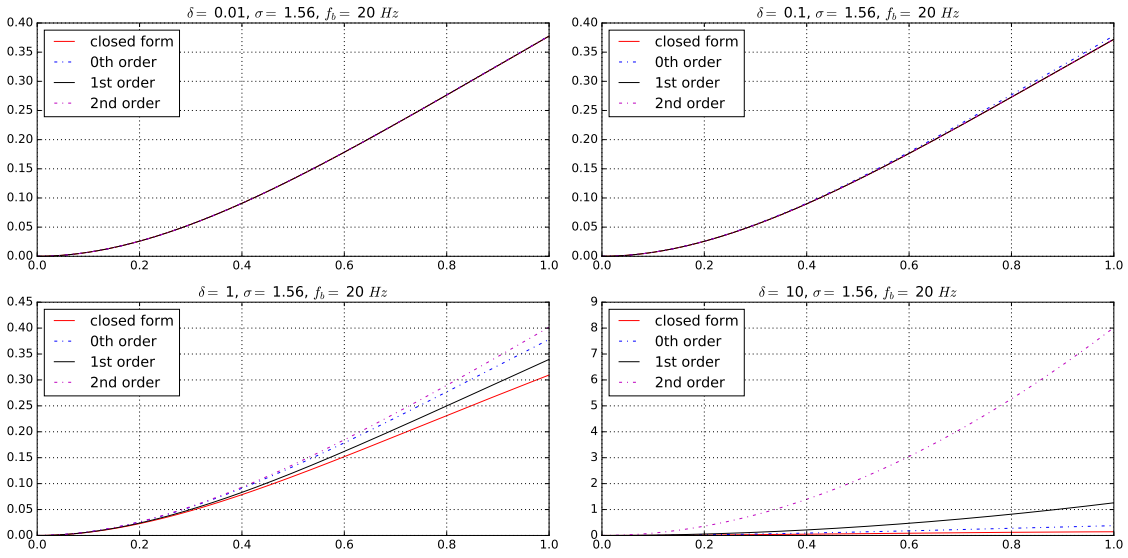

Figure 6: Comparison for the different orders of asymptotic expansion for the dimensionless relative displacement function $u_\delta(z)$.

This is exactly the displacement function of a pure elastic cantilever beam. It means that for

most piezoelectric energy harvesting devices, due to the fact that the electromechanical coupling factor is relatively small, the displacement function is not much affected. In this way, we have indeed uncoupled the electrical part and elastic part of a piezoelectric energy harvesting device. It should be noted that the approximation is not valid near the resonant points.

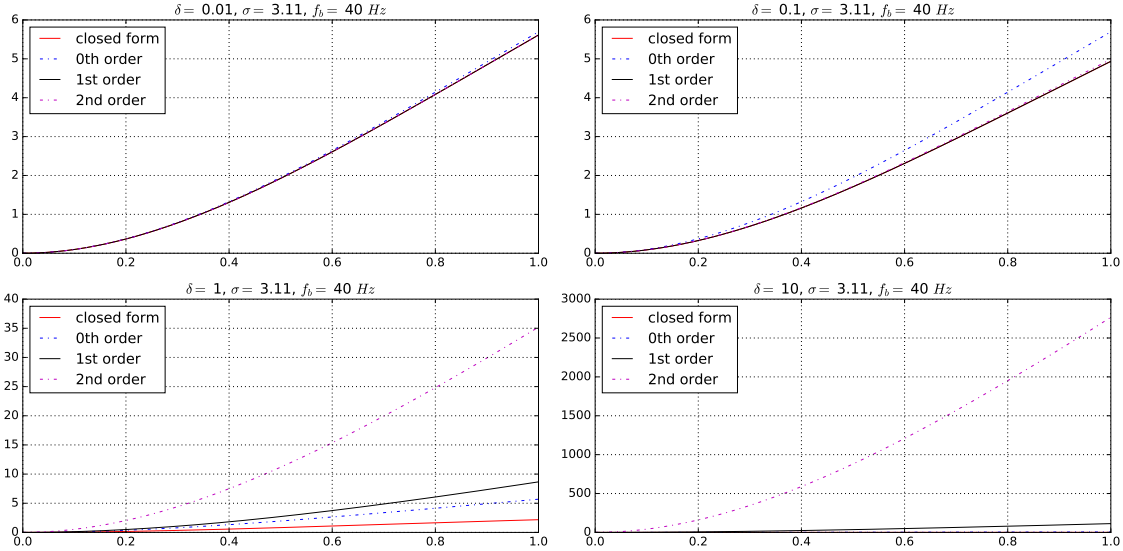

Figure 7: Comparison for the different orders of asymptotic expansion for the dimensionless relative displacement function $u_\delta(z)$.

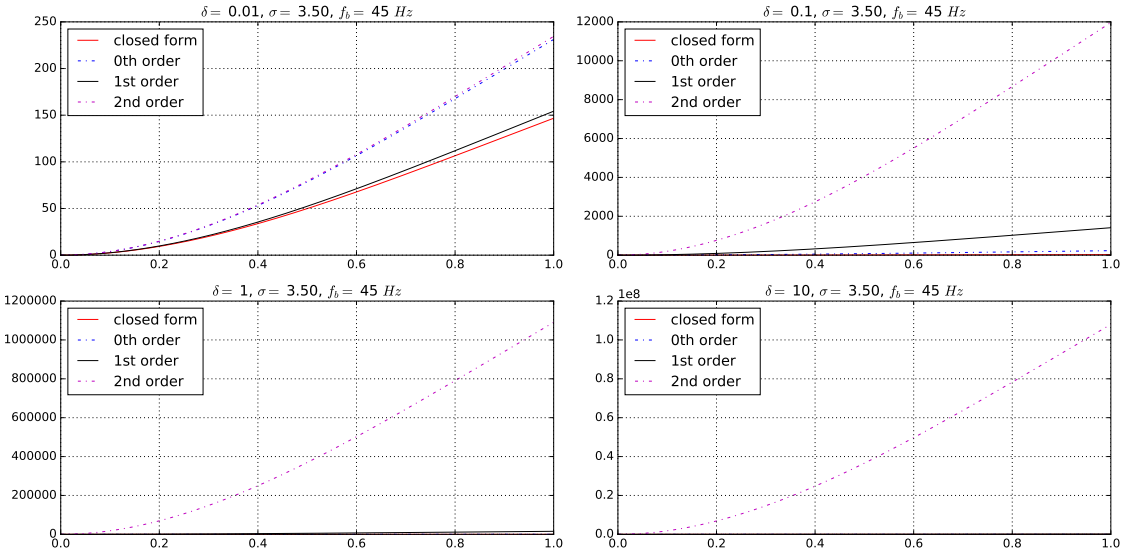

Figure 8: Comparison for the different orders of asymptotic expansion for the dimensionless relative displacement function $u_\delta(z)$.

Theoretically, the first order derivative of the dimensionless relative displacement funtion $u(z;\delta)$ is

$$u'(z;\delta) = \sigma^{1/2}\left(-A_\delta \sin\sqrt{\sigma}z + B_\delta \cos\sqrt{\sigma}z + C_\delta \sinh\sqrt{\sigma}z + D_\delta \cosh\sqrt{\sigma}z\right). \tag{42}$$

$$\chi_p = u_1'(1) = \frac{\sqrt{\sigma}\left(\sinh\sqrt{\sigma} - \sin\sqrt{\sigma}\right)}{1 + \cos\sqrt{\sigma}\cosh\sqrt{\sigma} + \frac{j\beta\sqrt{\sigma}}{1+j\beta\sigma}\delta\left(\cos\sqrt{\sigma}\sinh\sqrt{\sigma} + \sin\sqrt{\sigma}\cosh\sqrt{\sigma}\right)}. \tag{43}$$

The value of this function at the free end ($z = 1$) is just the output index χ_p according to equation (29). To see the influences of δ and f_b, therefore σ, upon χ_p, we firslty calcualte the values of χ_p

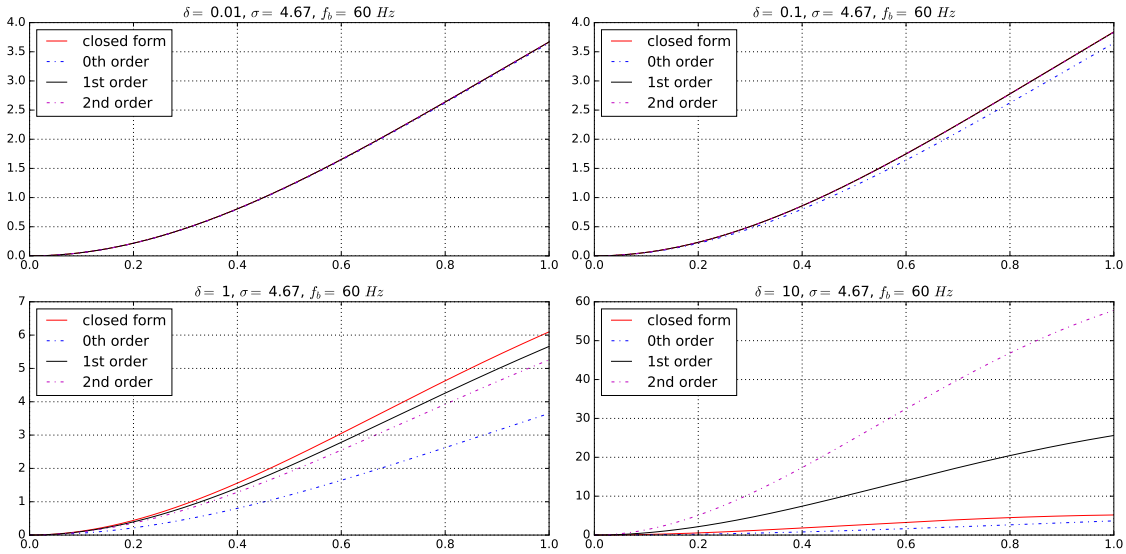

Figure 9: Comparison for the different orders of asymptotic expansion for the dimensionless relative displacement function $u_\delta(z)$.

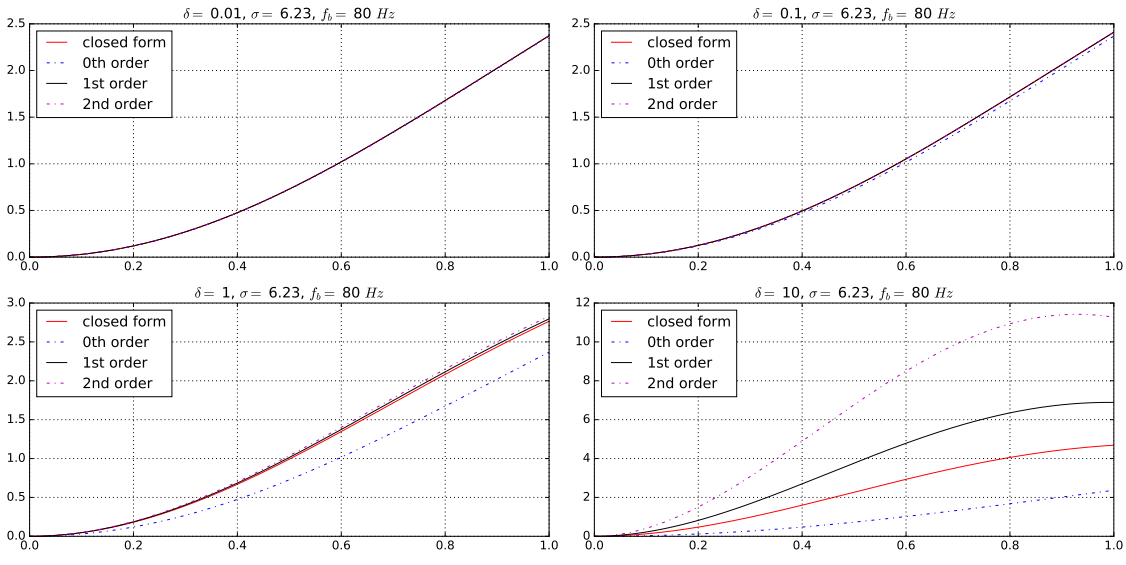

Figure 10: Comparison for the different orders of asymptotic expansion for the dimensionless relative displacement function $u_\delta(z)$.

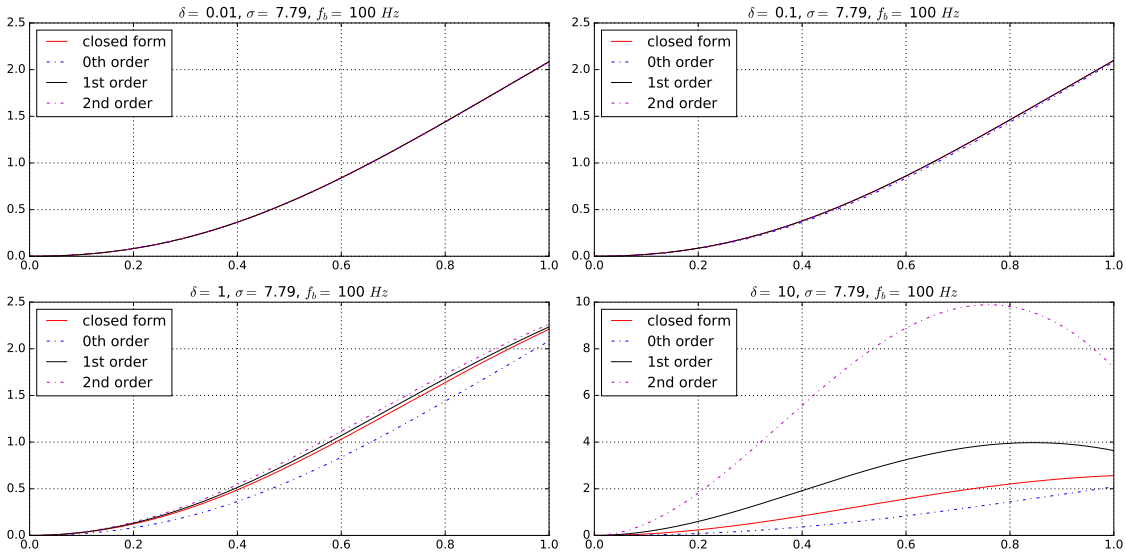

Figure 11: Comparison for the different orders of asymptotic expansion for the dimensionless relative displacement function $u_\delta(z)$.

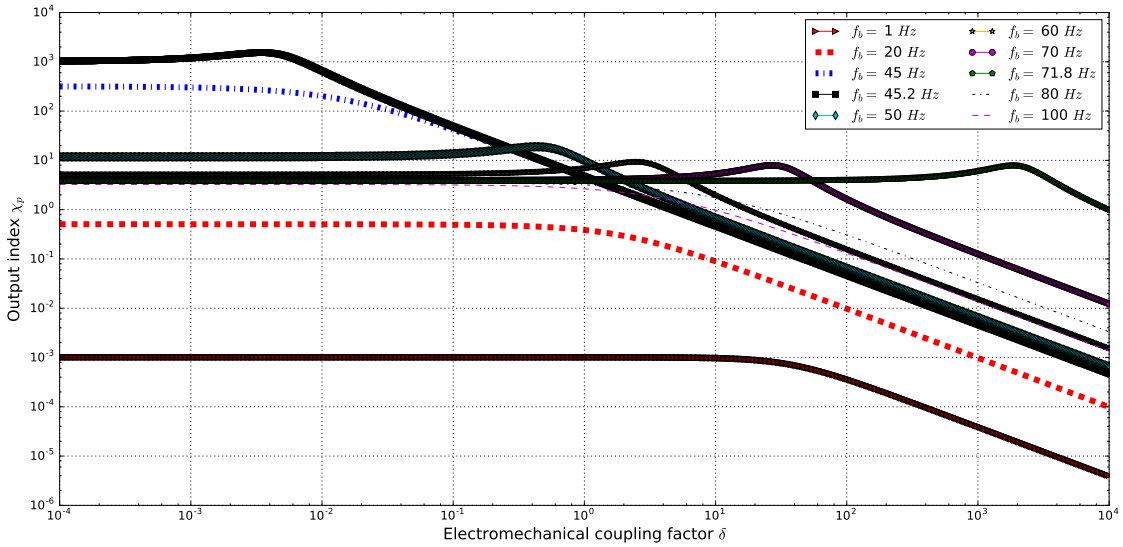

Figure 12: Output index χ_p as a function of electromechanical coupling factor δ at different values of base excitation frequency f_b.

for different values of δ by fixing the value of f_b to be some discrete values. The results are shown in Figure 12.

It is seen that the dependence of χ_p upon δ shows two different modes in the frequency range of $1 - 100\ Hz$. For the frequencies of $45.2\ Hz \leq f_b \leq 71.8\ Hz$, a peak corresponding to a critical value of δ_p is present in the considered range of δ. When δ is smaller than δ_p, the output index χ_p increases along with δ, and when δ is larger than δ_p, the output index χ_p decreases with the increase of δ. On the other hand, for the frequency range of $f_b \leq 45\ Hz$ or $f_b \geq 80\ Hz$, the output index χ_p shows a monotonical decrease with respect to the increase δ.

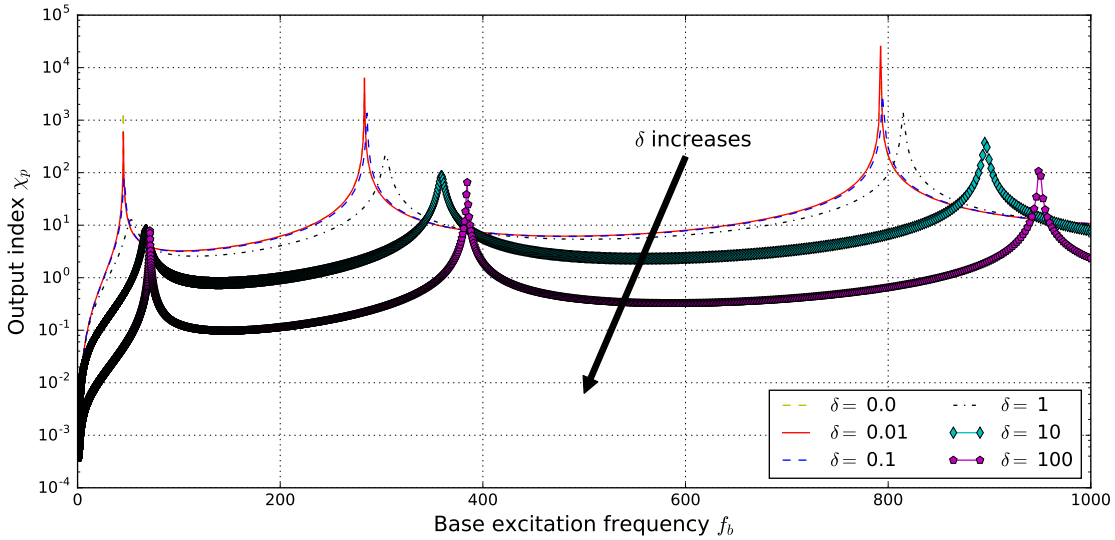

Figure 13: Output index χ_p as a function of base excitation frequency f_b at different values of electromechanical coupling factor δ.

Alternatively, by fixing the values of δ to a discrete set of numbers, we calculate the values of χ_p in relation to different values of f_b. This is very similar to a frequency response of the output index as a function of σ. The results are shown in Figure 13. It is clearly shown that with the increase of electromechanical coupling factor δ, the resonant frequencies to the system increase with the increase of δ. This is clearly shown in the shift to the right of the frequency response curve. Besides, we add in this figure the case where $\delta = 0.0$ as a reference. Simple comparisons show that the discrepency between the frequency response curves related to the case of $\delta = 0$, $\delta = 0.01$, and $\delta = 0.1$ is small. A direct conclusion is that for relatively small values of electromechanical coupling factor δ, the output index χ_p can be approximated by

$$\chi_p \approx \frac{\sqrt{\sigma}\left(\sinh\sqrt{\sigma} - \sin\sqrt{\sigma}\right)}{1 + \cos\sqrt{\sigma}\cosh\sqrt{\sigma}}. \tag{44}$$

As a result, the output performance measures $\tilde{V}_p$, $\tilde{I}_p$, and $\tilde{P}_p$ can be approximated by

$$\begin{cases} \tilde{V}_p = -\dfrac{j\sigma\beta}{j\sigma\beta+1}\left(\dfrac{\eta_b}{l_p}\right)\left(\dfrac{e_p}{C_p}\right)\chi_p, \\ \quad = -\dfrac{j\sigma\beta}{j\sigma\beta+1}\left(\dfrac{\eta_b}{l_p}\right)\left(\dfrac{e_p}{C_p}\right)\dfrac{\sqrt{\sigma}\left(\sinh\sqrt{\sigma} - \sin\sqrt{\sigma}\right)}{1 + \cos\sqrt{\sigma}\cosh\sqrt{\sigma}}, \\ \tilde{I}_p = \tilde{V}_p/R_l = -\dfrac{j\sigma\beta}{j\sigma\beta+1}\left(\dfrac{\eta_b}{l_p}\right)\left(\dfrac{e_p}{C_pR_l}\right)\chi_p, \\ \quad = -\dfrac{j\sigma\beta}{j\sigma\beta+1}\left(\dfrac{\eta_b}{l_p}\right)\left(\dfrac{e_p}{C_pR_l}\right)\dfrac{\sqrt{\sigma}\left(\sinh\sqrt{\sigma} - \sin\sqrt{\sigma}\right)}{1 + \cos\sqrt{\sigma}\cosh\sqrt{\sigma}}, \\ \tilde{P}_p = \tilde{V}_p^2/R_l = \left(\dfrac{\eta_b}{l_p}\right)^2\left(\dfrac{e_p}{C_p}\right)\left(\dfrac{e_p}{C_pR_l}\right)\left(\dfrac{j\sigma\beta}{j\sigma\beta+1}\right)^2\chi_p^2, \\ \quad = \left(\dfrac{\eta_b}{l_p}\right)^2\left(\dfrac{e_p}{C_p}\right)\left(\dfrac{e_p}{C_pR_l}\right)\left(\dfrac{j\sigma\beta}{j\sigma\beta+1}\right)^2\left(\dfrac{\sqrt{\sigma}\left(\sinh\sqrt{\sigma} - \sin\sqrt{\sigma}\right)}{1 + \cos\sqrt{\sigma}\cosh\sqrt{\sigma}}\right)^2. \end{cases} \tag{45}$$

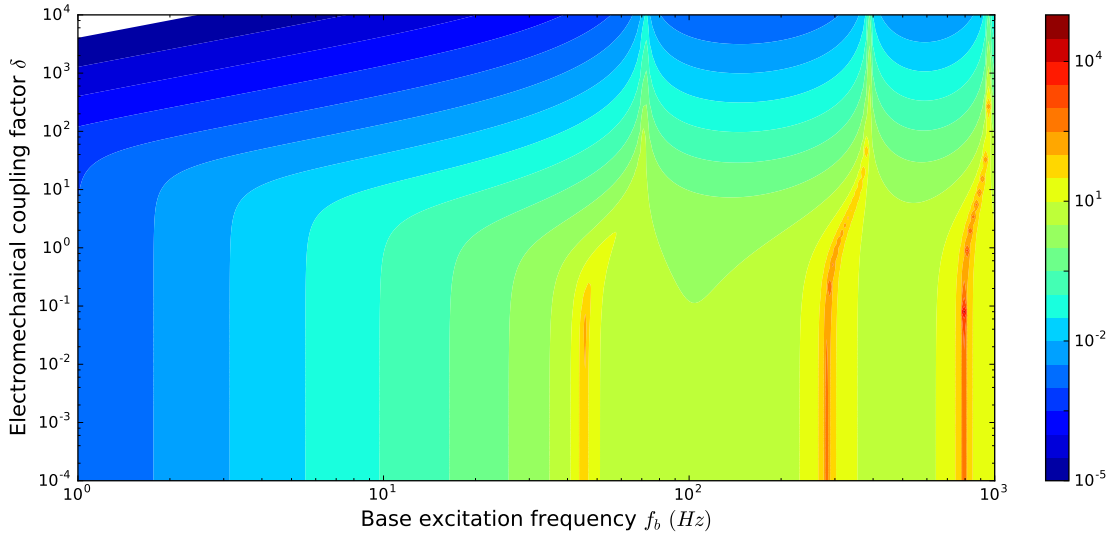

Figure 14: Output index χ_p as a function of base excitation frequency f_b and electromechanical coupling factor δ.

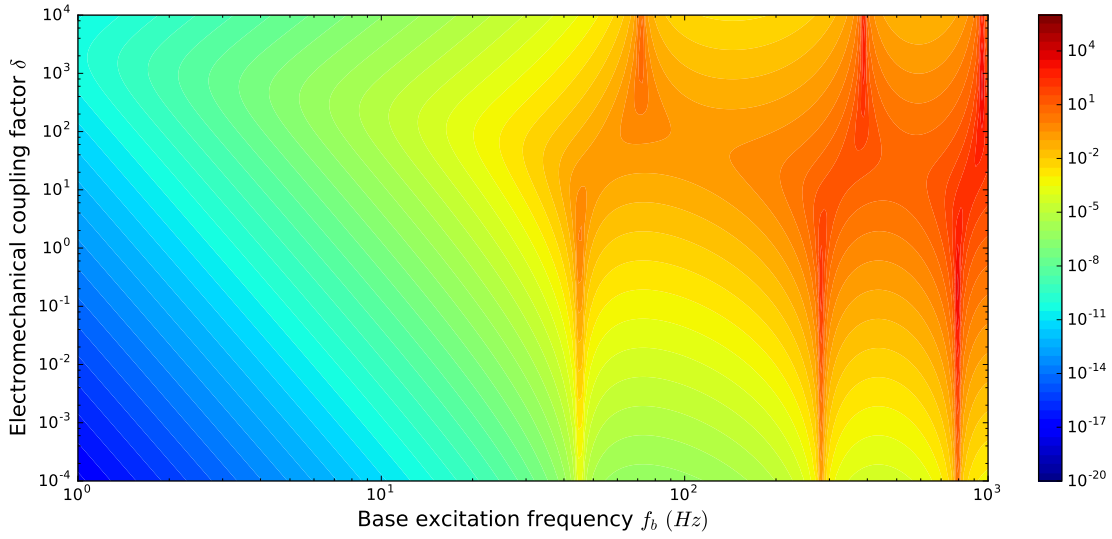

Figure 15: Output voltage $\tilde{V}_p$ as a function of base excitation frequency f_b and electromechanical coupling factor δ.

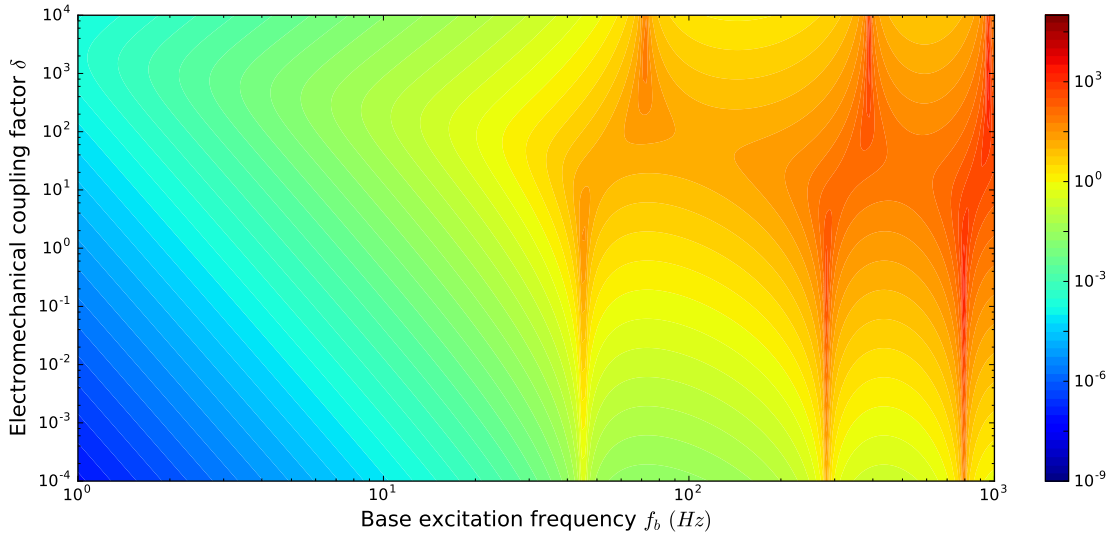

Figure 16: Output voltage $\tilde{P}_p$ as a function of base excitation frequency f_b and electromechanical coupling factor δ.

6 Conclusion

Appendices

The asymptotic expansion of equation (23) can be found using an iterative method. In fact, for higher order expansions ($k \geq 1$), we have the following iterative relation:

$$\begin{cases} A_{k+1} + C_{k+1} = 0, \\ B_{k+1} + D_{k+1} = 0, \\ \left(-A_{k+1}\cos\sqrt{\sigma} - B_{k+1}\sin\sqrt{\sigma} + C_{k+1}\cosh\sqrt{\sigma} + D_{k+1}\sinh\sqrt{\sigma}\right) + \\ \dfrac{j\beta\sqrt{\sigma}}{j\sigma\beta+1}\left(-A_k\sin\sqrt{\sigma} + B_k\cos\sqrt{\sigma} + C_k\sinh\sqrt{\sigma} + D_k\cosh\sqrt{\sigma}\right) = 0, \\ A_{k+1}\sin\sqrt{\sigma} - B_{k+1}\cos\sqrt{\sigma} + C_{k+1}\sinh\sqrt{\sigma} + D_{k+1}\cosh\sqrt{\sigma} = 0, \end{cases} \tag{46}$$

whose solution is expressed by

$$\begin{cases} A_{k+1} = \left(\dfrac{j\beta\sqrt{\sigma}}{1+j\beta\sigma}\right)\left(\dfrac{\cos\sqrt{\sigma}+\cosh\sqrt{\sigma}}{2\cos\sqrt{\sigma}\cosh\sqrt{\sigma}+2}\right)(Q_k), \\ B_{k+1} = \left(\dfrac{j\beta\sqrt{\sigma}}{1+j\beta\sigma}\right)\left(\dfrac{-\sinh\sqrt{\sigma}+\sin\sqrt{\sigma}}{2\cos\sqrt{\sigma}\cosh\sqrt{\sigma}+2}\right)(Q_k), \\ C_{k+1} = \left(\dfrac{j\beta\sqrt{\sigma}}{1+j\beta\sigma}\right)\left(-\dfrac{\cos\sqrt{\sigma}+\cosh\sqrt{\sigma}}{2\cos\sqrt{\sigma}\cosh\sqrt{\sigma}+2}\right)(Q_k), \\ D_{k+1} = \left(\dfrac{j\beta\sqrt{\sigma}}{1+j\beta\sigma}\right)\left(\dfrac{-\sin\sqrt{\sigma}+\sinh\sqrt{\sigma}}{2\cos\sqrt{\sigma}\cosh\sqrt{\sigma}+2}\right)(Q_k), \end{cases} \tag{47}$$

in which

$$Q_k = -A_k\sin\sqrt{\sigma} + B_k\cos\sqrt{\sigma} + C_k\sinh\sqrt{\sigma} + D_k\cosh\sqrt{\sigma}. \tag{48}$$

In terms of Q_k ($k \geq 0$), we have the following iterative relation

$$Q_{k+1} = -\left(\frac{\sin\sqrt{\sigma}\cosh\sqrt{\sigma}+\cos\sqrt{\sigma}\sinh\sqrt{\sigma}}{\cos\sqrt{\sigma}\cosh\sqrt{\sigma}+1}\right)\left(\frac{j\beta\sqrt{\sigma}}{1+j\beta\sigma}\right)Q_k, \tag{49}$$

and the initial two values Q_0 and Q_1:

$$\begin{cases} Q_0 = \dfrac{\sinh\sqrt{\sigma}-\sin\sqrt{\sigma}}{\cos\sqrt{\sigma}\cosh\sqrt{\sigma}+1}, \\ Q_1 = \dfrac{j\beta\sqrt{\sigma}}{1+j\beta\sigma}\left(\dfrac{\sin\sqrt{\sigma}-\sinh\sqrt{\sigma}}{\cos\sqrt{\sigma}\cosh\sqrt{\sigma}+1}\right)\left(\dfrac{\cos\sqrt{\sigma}\sinh\sqrt{\sigma}+\sin\sqrt{\sigma}\cosh\sqrt{\sigma}}{\cos\sqrt{\sigma}\cosh\sqrt{\sigma}+1}\right). \end{cases} \tag{50}$$

Hence it is shown that for $k \geq 0$,

$$Q_k = \left[-\left(\frac{j\beta\sqrt{\sigma}}{1+j\beta\sigma} \right) \left(\frac{\sin\sqrt{\sigma}\cosh\sqrt{\sigma} + \cos\sqrt{\sigma}\sinh\sqrt{\sigma}}{\cos\sqrt{\sigma}\cosh\sqrt{\sigma}+1} \right) \right]^k \left(\frac{\sinh\sqrt{\sigma} - \sin\sqrt{\sigma}}{\cos\sqrt{\sigma}\cosh\sqrt{\sigma}+1} \right). \tag{51}$$

As a result, we obtain that for $k \geq 1$,

$$\begin{cases} A_k = \left(\frac{j\beta\sqrt{\sigma}}{1+j\beta\sigma} \right)^k \left(\frac{-\sin\sqrt{\sigma}\cosh\sqrt{\sigma} - \cos\sqrt{\sigma}\sinh\sqrt{\sigma}}{\cos\sqrt{\sigma}\cosh\sqrt{\sigma}+1} \right)^{k-1} \left(\frac{\sinh\sqrt{\sigma} - \sin\sqrt{\sigma}}{\cos\sqrt{\sigma}\cosh\sqrt{\sigma}+1} \right) \left(\frac{\cos\sqrt{\sigma} + \cosh\sqrt{\sigma}}{2\cos\sqrt{\sigma}\cosh\sqrt{\sigma}+2} \right), \\ B_k = \left(\frac{j\beta\sqrt{\sigma}}{1+j\beta\sigma} \right)^k \left(\frac{-\sin\sqrt{\sigma}\cosh\sqrt{\sigma} - \cos\sqrt{\sigma}\sinh\sqrt{\sigma}}{\cos\sqrt{\sigma}\cosh\sqrt{\sigma}+1} \right)^{k-1} \left(\frac{\sinh\sqrt{\sigma} - \sin\sqrt{\sigma}}{\cos\sqrt{\sigma}\cosh\sqrt{\sigma}+1} \right) \left(\frac{-\sinh\sqrt{\sigma} + \sin\sqrt{\sigma}}{2\cos\sqrt{\sigma}\cosh\sqrt{\sigma}+2} \right), \\ C_k = \left(\frac{j\beta\sqrt{\sigma}}{1+j\beta\sigma} \right)^k \left(\frac{-\sin\sqrt{\sigma}\cosh\sqrt{\sigma} - \cos\sqrt{\sigma}\sinh\sqrt{\sigma}}{\cos\sqrt{\sigma}\cosh\sqrt{\sigma}+1} \right)^{k-1} \left(\frac{\sinh\sqrt{\sigma} - \sin\sqrt{\sigma}}{\cos\sqrt{\sigma}\cosh\sqrt{\sigma}+1} \right) \left(\frac{-\cos\sqrt{\sigma} - \cosh\sqrt{\sigma}}{2\cos\sqrt{\sigma}\cosh\sqrt{\sigma}+2} \right), \\ D_k = \left(\frac{j\beta\sqrt{\sigma}}{1+j\beta\sigma} \right)^k \left(\frac{-\sin\sqrt{\sigma}\cosh\sqrt{\sigma} - \cos\sqrt{\sigma}\sinh\sqrt{\sigma}}{\cos\sqrt{\sigma}\cosh\sqrt{\sigma}+1} \right)^{k-1} \left(\frac{\sinh\sqrt{\sigma} - \sin\sqrt{\sigma}}{\cos\sqrt{\sigma}\cosh\sqrt{\sigma}+1} \right) \left(\frac{-\sin\sqrt{\sigma} + \sinh\sqrt{\sigma}}{2\cos\sqrt{\sigma}\cosh\sqrt{\sigma}+2} \right). \end{cases}$$

Acknowledgements

References

[1] Beeby SP, Tudor MJ, White N. Energy harvesting vibration sources for microsystems applications. Measurement science and technology. 2006;17(12):R175.

[2] Anton SR, Sodano HA. A review of power harvesting using piezoelectric materials (2003–2006). Smart materials and Structures. 2007;16(3):R1.

[3] Zhou M, Al-Furjan MSH, Zou J, Liu W. A review on heat and mechanical energy harvesting from human–Principles, prototypes and perspectives. Renewable and Sustainable Energy Reviews. 2018;82:3582–3609.

[4] Safaei M, Sodano HA, Anton SR. A review of energy harvesting using piezoelectric materials: state-of-the-art a decade later (2008–2018). Smart Materials and Structures. 2019;28(11):113001.

[5] Roundy S, Wright PK, Rabaey J. A study of low level vibrations as a power source for wireless sensor nodes. Computer communications. 2003;26(11):1131–1144.

[6] Shu Y, Lien I. Analysis of power output for piezoelectric energy harvesting systems. Smart materials and structures. 2006;15(6):1499.

[7] Shu Y, Lien I, Wu W. An improved analysis of the SSHI interface in piezoelectric energy harvesting. Smart Materials and Structures. 2007;16(6):2253.

[8] Qiu J, Jiang H, Ji H, Zhu K. Comparison between four piezoelectric energy harvesting circuits. Frontiers of Mechanical Engineering in China. 2009;4(2):153–159.

[9] Erturk A, Inman DJ. A distributed parameter electromechanical model for cantilevered piezoelectric energy harvesters. Journal of vibration and acoustics. 2008;130(4):041002.

[10] Erturk A, Inman DJ. An experimentally validated bimorph cantilever model for piezoelectric energy harvesting from base excitations. Smart materials and structures. 2009;18(2):025009.